DOT/FAA/TC-17/56

Federal Aviation Administration
William J. Hughes Technical Center
Aviation Research Division
Atlantic City International Airport
New Jersey 08405

Stall Departure Identification, Recognition, and Recovery

March 2018

Final Report

U.S. Department of Transportation
Federal Aviation Administration

NOTICE

Technical Report Documentation Page

1. Report No.	2. Government Accession No.	3. Recipient's Catalog No.
DOT/FAA/TC-17/56		

4. Title and Subtitle	5. Report Date
STALL DEPARTURE IDENTIFICATION, RECOGNITION, AND RECOVERY	March 2018
	6. Performing Organization Code

7. Author(s)	8. Performing Organization Report No.
William (Bill) Gato, John T Tran, Frank R Brown	

9. Performing Organization Name and Address	10. Work Unit No. (TRAIS)
	11. Contract or Grant No.

12. Sponsoring Agency Name and Address	13. Type of Report and Period Covered
U.S. Department of Transportation FAA Northwest Mountain Regional Office Safety Management Section 1601 Lind Ave SW Renton, WA 98057	Final Report
	14. Sponsoring Agency Code AIR-677

15. Supplementary Notes

The FAA William J. Hughes Technical Center Aviation Research Division COR was Robert J. McGuire.

16. Abstract

Loss of Control (LOC) is one of the leading causes of commercial jet airplane fatalities worldwide. Stall departures are major contributors to LOC accidents. A congressional mandate in 2010 and a recent FAA ruling will require full-stall training in the near future. To address this type of training, flight-simulation training devices are being updated with higher fidelity stall and post-stall aerodynamics. The overall goal of this project was to provide guidelines for the cost-effective development of the aerodynamics modeling required to update these devices with the potential for expanded simulation capabilities beyond full-stall training. One such model was developed for the NASA Enhanced Upset Recovery Simulation (EURS). The EURS was the state-of-the-art standard and baseline for the research work in this project, which progressed in the following logical sequence:

- Develop means to quantitatively characterize and define stall departure characteristics.
- Assess the ability of the NASA EURS to reproduce any of these defined characteristics.
- Determine and rank the model parameters having the greatest impact on the identified departure characteristics and the sensitivity in modeling accuracy of these parameters.
- Assess the level of effort and the total cost required to develop an aerodynamics model for a similarly configured transport category airplane as that modeled by the EURS.

All project objectives were achieved in the above sequence. In the final assessment, three cost-benefit options were explored, weighing different proportions of wind-tunnel testing and analytical methods to develop the aerodynamics modeling required. All three options represent a significant reduction in the wind-tunnel test data used for the development of the EURS. One of the options is recommended since it offers acceptable accuracy at a reasonable combined cost of wind-tunnel testing, post-test processing analysis, data extrapolation through analytic methods guided by EURS trends, and aerodynamics model-building.

The insight gained in this project and the conclusions and recommendations put forth in this report can serve as a guide in developing the aerodynamics for flight simulators capable of sufficiently accurate representations of the stall and post-stall departure characteristics of a conventional twin-jet transport category airplane.

17. Key Words	18. Distribution Statement
Stall, Stall departure characteristics, Loss of Control, Aerodynamic Modeling, Flight simulators	This document is available to the U.S. public through the National Technical Information Service (NTIS), Springfield, Virginia 22161.

19. Security Classif. (of this report)	20. Security Classif. (of this page)	21. No. of Pages	22. Price
Unclassified	Unclassified	71	

ACKNOWLEDGEMENTS

The authors of this document would like to thank several people who contributed to the effort in a variety of ways. Dhar Patel and Doug Hansen aided in the research and analysis in the earlier phase. John Foster from NASA was a key resource for consulting on the EURS model. Leon Robert, Gerald (Jerry) Whites, and Dave Carbaugh, the pilots contributing to the project, all provided critical insight into the stall departures being sought and evaluated. General guidance and mentoring provided by Jia Luo and Dave Shikany also enabled the team to more easily work through the problems presented in this study. All of these people made both direct and indirect contributions that enabled the success of the effort.

TABLE OF CONTENTS

LIST OF FIGURES

LIST OF TABLES

LIST OF ACRONYMS

EURS	NASA Enhanced Upset Recovery Simulation
FDR	Flight data recorder
LaRC	NASA Langley Research Center
LOC	Loss of control
QSD	Quantitative Stall Departure

EXECUTIVE SUMMARY

A 2010 statistical summary by the Common Aviation Safety Team/International Civil Aviation Organization Common Taxonomy Team showed that loss of control was the leading cause of fatalities in the worldwide commercial jet fleet from 2001–2010, with stall departures being major contributors. Despite recent progress in reducing the occurrences of these departures, further reductions are sought through various means, one of them being stall recognition and avoidance training. A congressional mandate in 2010 and a recent FAA ruling will require full-stall training in the near future. To address this type of training, flight simulation training devices are being updated with higher fidelity stall and post-stall aerodynamics. The overall goal of this project was to provide guidelines for the cost-effective development of the aerodynamics modeling required to update these devices with the potential for expanded simulation capabilities beyond full-stall training. The research in this project leveraged existing industry and NASA data and methods in the development of enhanced models, which more accurately capture the aerodynamics of transport-category airplanes in the stall and post-stall flight regime. One such model was developed for the NASA Enhanced Upset Recovery Simulation (EURS). The EURS was the state-of-the-art standard and baseline for the research work in this project, which progressed in the following logical sequence:

- Develop means to quantitatively characterize and define stall departure characteristics.
- Assess the ability of the NASA EURS to reproduce any of these defined characteristics.
- Determine and rank the model parameters having the greatest impact on the identified departure characteristics, and assess the sensitivity in modeling accuracy of these parameters.
- Assess the level of effort and the total cost required to develop an aerodynamics model for a similarly configured transport category airplane as modeled by the EURS.

An extensive search of the public literature and engagement of the subject-matter experts at The Boeing Company revealed that a method to quantitatively characterize and define stall departure characteristics did not exist. However, there was sufficient insight gained and information gathered in this endeavor to develop such a method specifically for this project. The Quantitative Stall Departure (QSD) Definition Tree method is a process in which a path along logic-tree identifies patterns and relationships in value, sign, and vector orientation of pertinent flight or simulation parameters. These patterns and quantitative relationships, and the logic paths traced throughout the time history of a stall departure, together characterize and define the individual aspects of the departure and the sequence in which they occur.

A multitude of stall maneuvers in desktop and pilot-in-the-loop simulations revealed two major stall-departure characteristics of the EURS as determined through the QSD defining process: yaw departures and roll departures. Several individual aspects of these two departure characteristics were identified. Nose-slice and roll-off aspects were identified in the initial phase of the stall departure. In the fully developed phase, a spiral/spin aspect was identified with a superimposed oscillatory wing-rock aspect. Both of these fully developed post-stall departure aspects differed depending on the presence or absence of aggravating control inputs—in one case changing into a falling-leaf departure and in another changing into post-stall gyrations.

All the moment parameters in the EURS aerodynamics model, as a group, had the greatest impact on the simulation fidelity of these departure aspects. They were individually ranked according to the magnitude of their effect on simulation fidelity. The sensitivity in simulation fidelity to reductions in data range, density, and value accuracy of these parameters defined the required minimums for the development of an aerodynamics model for a similarly configured transport category airplane as that modeled by the EURS.

Three cost-benefit options were explored, weighing different proportions of wind-tunnel testing and analytical methods to develop the aerodynamics modeling required. All three options represent a significant reduction in the wind-tunnel test data used in the development of the EURS. One of the options is recommended because it offers acceptable accuracy at a reasonable combined cost of wind-tunnel testing, post-test processing analysis, data extrapolation, and aerodynamics model-building.

The insight gained in this project and the conclusions and recommendations put forth in this report can serve as a guide in developing the aerodynamics for flight simulators capable of sufficiently accurate representations of the stall and post-stall departure characteristics of a conventional twin-jet transport category airplane.

1. INTRODUCTION

A large percentage of aviation fatalities is attributed to loss of control (LOC) accidents. A 2010 statistical summary by the Common Aviation Safety Team/International Civil Aviation Organization Common Taxonomy Team showed that LOC was the leading cause of fatalities in the worldwide commercial jet fleet from 2001–2010, with approximately 42% more fatalities than the next leading cause of fatalities, namely controlled flight into terrain [1]. Stall and departure from controlled flight are major contributors to LOC accidents, resulting in more than 300 fatalities during that time period. Although technology advancements have been successful in predicting and reducing the occurrence of stalls and departures, advancements are needed to further reduce stall/departure occurrences [2].

The Next Generation National Airspace System is envisioned to provide a safe, efficient, and reliable air transportation system for 2025, delivering a system capacity that is up to three times that of current operating levels [3]. The primary goal of the research work aimed at further reducing the occurrence of stalls and departures by leveraging existing industry/NASA data and research methods to develop enhanced aerodynamic models. These models can then be used to simulate full-stall departure characteristics for various transport category airplanes and flight conditions. The results of this work can be used to develop advanced flight simulation models capable of supporting flight-crew training in the recognition and recovery from a full stall, which directly supports requirements currently in work by the Human Factors and the Terminal Area Safety Technical Committee Research Groups.

This research project delved into all aspects of stall and post-stall departure in transport category airplanes from descriptions and categorizations to more specific discriminators or criteria that can be quantified by way of basic flight parameters found in either conditioned flight-test or flight data recorder (FDR) datasets. The project had four distinct objectives, each associated with a separate task:

Phase 1

- Task 1 – Develop the criteria to quantitatively characterize and define stall departure characteristics for transport category airplanes.
- Task 2 – Assess the ability of a state-of-the-art stall simulation—the NASA Enhanced Upset Recovery Simulation (EURS)—to reproduce any of the stall departure characteristics defined in Task 1.

Phase 2

- Task 1 – Determine which components/parameters in the EURS aerodynamics model are primarily responsible for reproducing the departure characteristics found and the sensitivity of the simulated departures to their modeling accuracy.
- Task 2 – Assess the level of effort required to develop an aerodynamic model for a similarly configured airplane as that modeled by the EURS and the total cost of the associated analysis or wind-tunnel testing.

This report summarizes the research work in all phases of the entire project, including key results and recommendations. The report focuses on Phase 2 and Task 2, particularly where a road map for developing an EURS-like aerodynamics model for a similarly configured transport airplane was defined.

2. SUMMARY OF PHASE 1

The primary objective of the first phase in this research project was to determine the stall and post-stall departure characteristics exhibited by the prototype EURS provided by the NASA Langley Research Center (LaRC). A two-step process was followed in which criteria to quantitatively categorize and define all aspects of these departure characteristics were developed in Task 1. These definitions would characterize a specific departure aspect based on the quantitative values of basic flight-data parameters generally available in simulation data-stream output or in FDR. In Task 2, these same definitions were applied to data from almost 300 desktop simulations across a wide spectrum of stall maneuvers designed to reveal all stall and post-stall departure behaviors exhibited by the EURS. Pilot-in-the-loop simulations followed to verify and expand on the desktop simulation findings.

2.1 CRITERIA DEVELOPMENT TO QUANTITATIVELY CATEGORIZE AND DEFINE STALL DEPARTURE CHARACTERISTICS

The following six stall-departure characteristics provided the starting point for the development of quantitative criteria, metrics, or a process that could be used to categorize a stall departure by one or more of these:

1. Nose-slice, yaw, or both
2. Wing drop or roll-off greater than 20º
3. Pitch-up not readily arrested by application of nose-down control inputs
4. Coupled oscillatory roll and yaw motions unaffected by lateral and directional control inputs (e.g., falling leaf)
5. Nonlinear control responses or reversals
6. Spin

On certified transport category airplanes, most of these characteristics may occur only when there is substantial penetration into the post-stall regime. The depth of this penetration will determine the nature of the stall departure and how many of the six departure characteristics manifest themselves if the airplane is susceptible to exhibiting them. In general, this susceptibility is closely linked to the configuration-dependent aerodynamics of the airplane and its mass properties. Pilot control inputs may be contributing factors or, in some cases, may cause the substantial penetration into the post-stall regime in which the susceptibility to any of these departure characteristic exists.

The expectation was that a thorough review of available literature would uncover additional departure characteristics and, more importantly, ways to quantitatively characterize them into a comprehensive definition of stall departure in all its manifestations. If such quantitative criteria were not found for any or all of the six departure characteristics, a thorough survey would still provide an understanding of the current state of the research in the subject of stall departure and its characterization. The process of developing a comprehensive definition of stall departure in quantitative terms would then become one of turning all the information gathered from the public literature and other sources into a descriptive catalogue of stall departure. Parametric information with enough relational detail could be organized in a definition process where specific aspects of stall departure could be characterized by linking them to patterns and relationships between the values of basic flight parameters. The compilation of the patterns and relationships for a particular

stall-departure characteristic in any of its aspects would, in essence, become its quantitative definition.

The public literature search identified several different aspects of the six departure characteristics (figure 1).

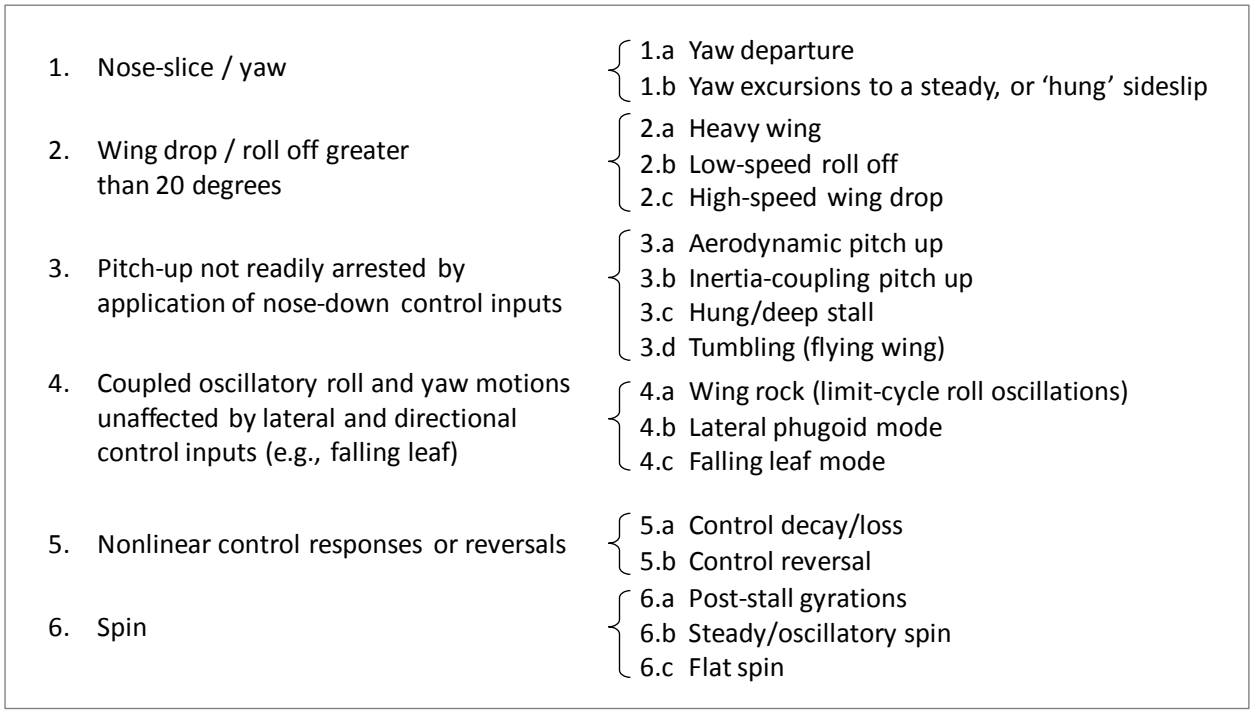

Figure 1. Expanded aspects of the six basic stall departure characteristics

The public literature search, however, did not reveal criteria sufficient to categorize and quantify stall-departure characteristics for transport-category airplanes. Engaging the relevant subject-matter experts at Boeing yielded similar results—qualitative descriptions but no quantifiable means of defining stall departure from basic flight-test or FDR parameters. Available transport airplane flight-test data were searched for examples with significant penetrations beyond stall to develop the quantitative database for this task. Only a few cases were found that could be confidently used to quantify one or two of the above specific stall-departure characteristics. However, there were no available data for some of those usually associated with deep, post-stall penetrations.

With the absence of existing criteria and very limited data on stall departures, the quantitative LOC methodology [4] was initially considered as a starting point for developing measurable criteria applicable to the identification and definition of stall-departure characteristics. While this methodology showed promise, extensive modifications would be required to give it the capability of differentiating between LOC events in general and a stall departure in particular. Both the development of the required modifications, which included introduction of a time element, and recalibrating the methodology with limited stall-departure data were deemed out of scope. The scarcity of quantitative data related to stall departures was overcome by the alternate approach developed specifically for this project. As conceptualized, this alternate approach would not

entirely rely on the values of basic flight parameters but on how these values related to each other across a group of basic flight parameters. These relationships would include the relative magnitude and sign; the relative direction of rotational and velocity vectors; the steady, oscillatory, or random character of the motions; and the relative contribution of derived components of some of the basic flight parameters. This approach, coined "The Quantitative Stall Departure (QSD) Definition Tree," was developed based on the body of knowledge gleaned from the literature and Boeing's experience on the subject. A portion of the definition process represented by this approach is notionally illustrated as a flow chart in figure 2.

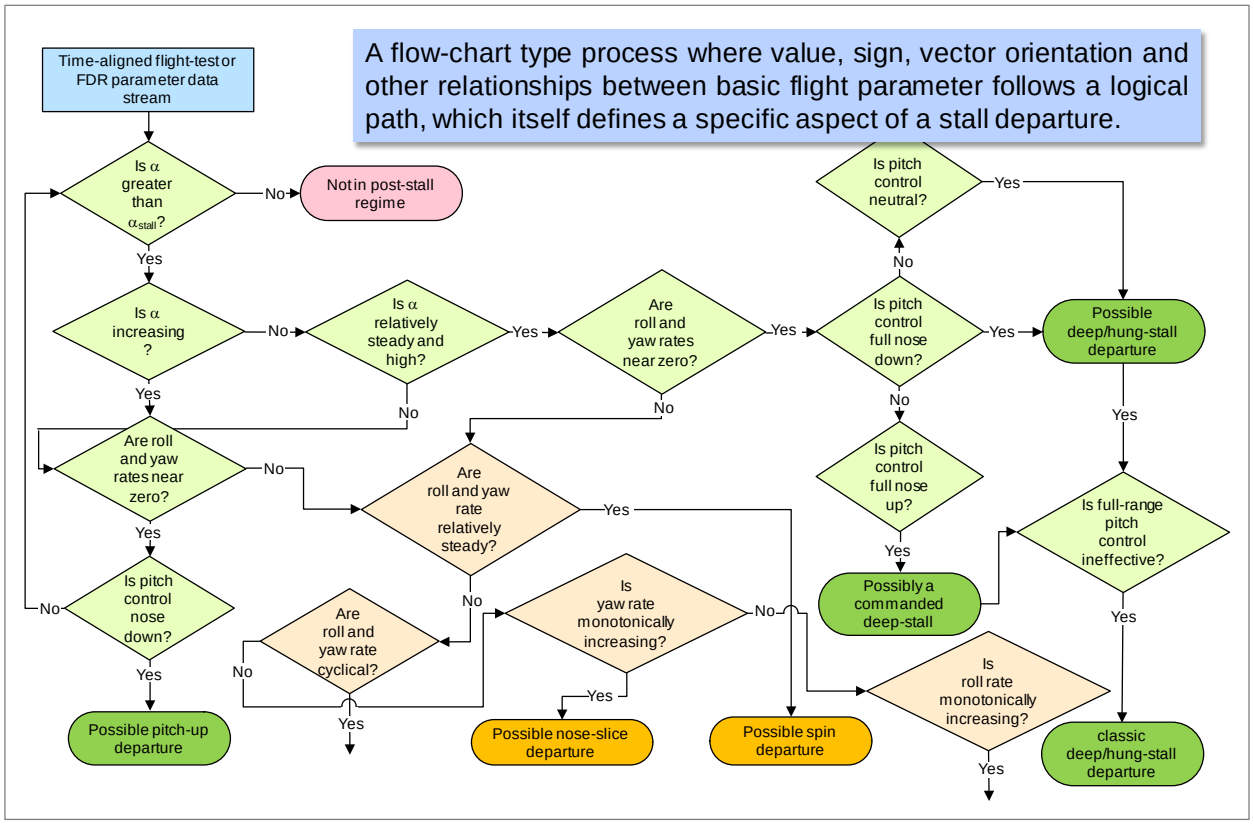

Figure 2. Notional QSD definition tree

A multitude of logic paths along intertwining question-and-answer branches lead to a selection of the possible stall-departure characteristics and their different aspects listed in figure 1. At some initial point in the time history of a stall departure, answers to a series of questions may lead along a particular path identifying one of these aspects. In this flow of questions and answers as to the values, signs, and other discriminators relating a group of parameters, the path traced, in essence, becomes the quantitative definition of the stall-departure aspects identified. However, a "no" answer to any of the questions in the series may lead to new branches that in turn may lead to one or more stall-departure characteristics and their various aspects. These may be sequential or concurrent in the initial phase of the stall departure, transitioning to a different aspect of the same departure characteristic in the fully developed phase or a different departure characteristic overall. It is possible that a stall departure does not have a fully developed phase if an early recovery from the stall departure is successful. Some of the fully developed post-stall departures, such as spins or a falling leaf, may not be present if the aerodynamics and mass properties of the airplane or

pilot-control inputs are not conducive to it. Consistent looping along the same path as the search through the time sequence continues will more definitively identify a departure characteristic in a portion of the time history. Branching off on a new path would indicate the development of a different stall-departure characteristic. Branches extending beyond the bottom of the page lead to additional departure aspects not shown. All paths should loop back to the top so that a "not in stall/post-stall regime" exit is possible when a recovery is achieved or, if not, so the search can then loop back and continue through the same path if a fully developed post-stall departure persists. Back tracking in time may be necessary to examine the period before the stall angle of attack is exceeded to ensure that stall approach behaviors leading to the post-stall departure are detected. A strip chart view of the parameter time histories may be helpful to identify a particular stall-departure type, such as the falling leaf in which large, cyclical, and out-of-phase variations in angle of attack and sideslip, in a prescribed ratio, are a defining pattern/relationship of this departure aspect.

This notional definition process was subdivided into three different stall phases: initial, post-stall gyrations, and fully developed. The type of the departures was categorized in the initial phase by the axis of the dominant rotational motion. In the fully developed phase, particularly for steady-state departures, such as a hung stall or hung sideslip, the type of departure was categorized by the rotational motion typically leading to it.

In the initial phase, one aspect of a stall-departure characteristic could directly transition into the fully developed phase aspect of the same departure characteristic or transition to a different fully developed phase aspect—an altogether different aspect—after going through the post-stall-gyrations phase. The initial phase is characterized by monotonically increasing or decreasing changes in the values of related flight parameters, possibly with an oscillatory component. Flight parameter values in the fully developed phase are either steady state or changing in an oscillatory, limit-cycle manner that is repeatable. The post-stall-gyrations phase can be transitional or may persist without leading to the fully developed phase characterized by random changes in parameter value.

The notional question-and-answer flow was developed from a mapping of parameter value, sign, and vector relationships attributed to a specific aspect of a stall-departure characteristic in one of these phases. One such mapping, representative of the QSD definition for a spin, is presented in figure 3.

Attributes and Parameter Relationships for a Yaw Departure in the Fully Developed Stall Phase: A Spin

- Post-stall gyrations are less random and more spin-like (incipient spin phase) approaching a more stabilized dynamic phase
- An initial directional departure may lead to the incipient spin phase, sometimes oscillatory
- Angle of attack is high and nearly steady, and for airplanes with a high ratio of yaw-to-roll inertia, angle of attack is very high and the spin is flatter (flat spin)
- yaw and roll accelerations are near zero
- yaw and roll rates are substantial, of the same sign, and nearly steady with yaw rates higher for flatter spins
- Pitch rate, bank angle, and sideslip angle are small
- The rotational vector is nearly aligned with the velocity vector (same direction), which implies a steady wind-axes roll (or stability-axes if sideslip is near zero)
- The velocity vector points down (aligned with the z earth-axis)
- The rate of change of heading angle (turn rate) is nearly steady
- All of the above may have an oscillatory component from body-axes roll oscillations in which case the spin is oscillatory
- Airspeed is much lower than stall speed, and high rate of descent/altitude-loss
- Roll/yaw Inertia coupling and thrust effects balance the aerodynamic nose-down moment

Figure 3. Quantitative definition of a spin or fully developed yaw departure

An illustrative time-history of a flat spin [5] is presented in figure 4.

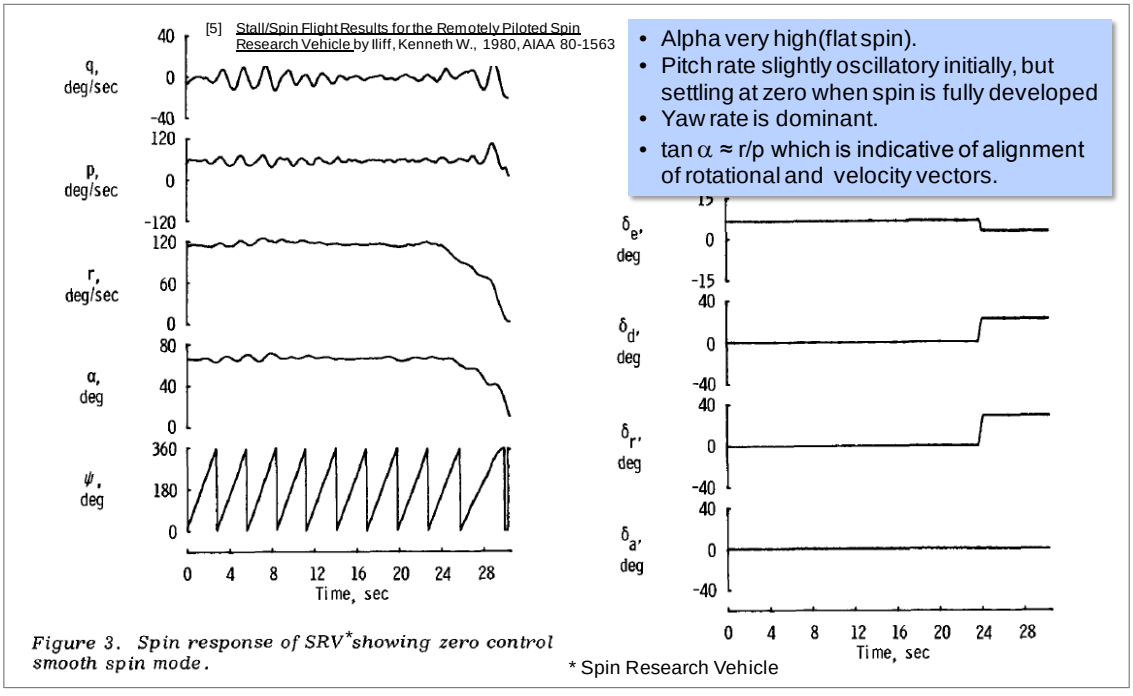

Figure 4. Example of parameter attributes and relationships for a flat spin

Quasi-quantitative definitions were developed for all six stall departure characteristics and some of their different aspects. These definitions were primarily based on descriptions and corresponding flight data found in the literature, such as that presented in figure 4. The few applicable examples of stall departures found in Boeing's flight test data archives provided insight for the more typical aspects in the initial phase of a stall departure: nose slice, roll off, and pitch up. The definitions for departure aspects in the fully developed phase, such as the hung stall, spin, and falling leaf were entirely based on descriptive information and data found in the literature. These definitions were conceptual and represented a first attempt at quantitatively characterizing the different aspects of a stall departure. However, with the absence of existing quantitative criteria in either public or internal domains, it was deemed the best candidate method for further development and application in Task 2.

2.2 ASSESSMENT OF THE STALL DEPARTURE CHARACTERISTICS IN THE NASA ENHANCED UPSET RECOVERY SIMULATION

The assessment of the capability of the EURS to reproduce any of the departure characteristics as conceptually defined in Task 1 by the QSD definition process was achieved through two major efforts:

1. Desktop simulations were conducted across a wide spectrum of stall maneuvers designed to reveal all stall and post-stall departure aspects exhibited by the EURS.
2. Pilot-in-the-loop simulations repeated the more significant of the desktop simulation stall maneuvers; and, as suggested by the group of expert test pilots, additional maneuvers were included to further explore the exhibited departure aspects and search for others not revealed by the desktop simulations.

The desktop simulation focused on the flaps-up configuration at a light weight and at the aft CG limit. A total of 297 variations of 77 stall maneuvers were analyzed with a limited number of them at a forward CG and at the takeoff flap deflection. Figure 5 captures the initial set of the stall maneuvers for the flaps-up configuration, which was expanded based on observations as the assessment proceeded. All stalls were at idle power to intentionally focus on the aerodynamics modeling of the EURS.

Man. #	Priority	Broad Categorization	Stall Maneuver Description	Flap Detent	Weight (lb)	CG (%)
1	1	Nominal wings-level stall	1 kt/sec. to aft column stop and release	0	184,000	39
2	2	Nominal wings-level stall	1 kt/sec. hold aft column for 2 sec. and release	0	184,000	39
3	1	Nominal wings-level stall	1 kt/sec. hold aft column for 5 sec. and release	0	184,000	39
4	2	Nominal wings-level stall	1 kt/sec. hold aft column for 15 sec. and release	0	184,000	39
5	1	Nominal wings-level stall	1 kt/sec. hold aft column for 40 sec. and release	0	184,000	39
6	1	Nominal wings-level stall	3 kt/sec. to aft column stop and release	0	184,000	39
7	2	Nominal wings-level stall	3 kt/sec. hold aft column for 2 sec. and release	0	184,000	39
8	1	Nominal wings-level stall	3 kt/sec. hold aft column for 5 sec. and release	0	184,000	39
9	2	Nominal wings-level stall	3 kt/sec. hold aft column for 15 sec. and release	0	184,000	39
10	1	Nominal wings-level stall	3 kt/sec. hold aft column for 60 sec. and release	0	184,000	39
11	1	Nominal turning stall	1 kt/sec. to aft column stop and release	0	184,000	39
12	2	Nominal turning stall	1 kt/sec. hold aft column for 2 sec. and release	0	184,000	39
13	1	Nominal turning stall	1 kt/sec. hold aft column for 5 sec. and release	0	184,000	39
14	2	Nominal turning stall	1 kt/sec. hold aft column for 15 sec. and release	0	184,000	39
15	1	Nominal turning stall	1 kt/sec. hold aft column for 40 sec. and release	0	184,000	39
16	1	Nominal turning stall	3 kt/sec. to aft column stop and release	0	184,000	39
17	2	Nominal turning stall	3 kt/sec. hold aft column for 2 sec. and release	0	184,000	39
18	1	Nominal turning stall	3 kt/sec. hold aft column for 5 sec. and release	0	184,000	39
19	2	Nominal turning stall	3 kt/sec. hold aft column for 15 sec. and release	0	184,000	39
20	1	Nominal turning stall	3 kt/sec. hold aft column for 60 sec. and release	0	184,000	39
21	1	Wings-level stall - slow column pull	3 kt/sec. pull 20 sec. to aft stop and hold for 40 sec.	0	184,000	39
22	2	Wings-level stall - nominal column pull	3 kt/sec. pull 5 sec. to aft stop and hold for 50 sec.	0	184,000	39
23	1	Wings-level stall - fast column pull	3 kt/sec. pull 2 sec. to aft stop and hold for 50 sec.	0	184,000	39
24	1	Wings-level stall - slow col-pull & lat-pulse	3 kt/sec. slow to aft stop hold & add full right wheel pulse at stall	0	184,000	39
25	1	Wings-level stall - slow col-pull & lat-pulse	3 kt/sec. slow to aft stop hold & add full right wheel pulse during pull	0	184,000	39
26	1	Wings-level stall - slow col-pull & lat-pulse	3 kt/sec. slow to aft stop hold & add full right wheel pulse at aft stop	0	184,000	39
27	1	Wings-level stall - slow col-pull & lat-step	3 kt/sec. slow to aft stop hold & add full right wheel step during pull	0	184,000	39
28	1	Wings-level stall - slow col-pull & lat-step	3 kt/sec. slow to aft stop hold & add full right wheel step at aft stop	0	184,000	39
29	1	Wings-level stall - slow col-pull & dir-pulse	3 kt/sec. slow to aft stop hold & add full left rudder pulse at stall	0	184,000	39

Figure 5. Simulation matrix of stall maneuvers for the desktop assessment

Basic flight parameter data and a number of derived parameters from these simulations were plotted in time-history and cross-plot formats. Some of the derived parameters, which were part of the definition process, included aerodynamic; thrust and inertia-coupling accelerations; and the kinematic-coupling and flight-path components contributing to the rate of change of angle of attack and sideslip and their integrated values. The character of the simulation traces in cross plots of angle of attack and sideslip were discriminators between the wing-rock, oscillatory-spiral/spin, and falling-leaf departure aspects in the fully developed phase. Similarly, roll rate vs. yaw rate and aero-propulsion vs. inertia-coupling pitch accelerations cross plots were used in the identification of fully developed spin-like departures. Eight different plot templates or summaries with up to 12 time history plots or 8 parameter cross-plots were designed to facilitate the application the QSD definition process, as illustrated in the simplified schematic in figure 6.

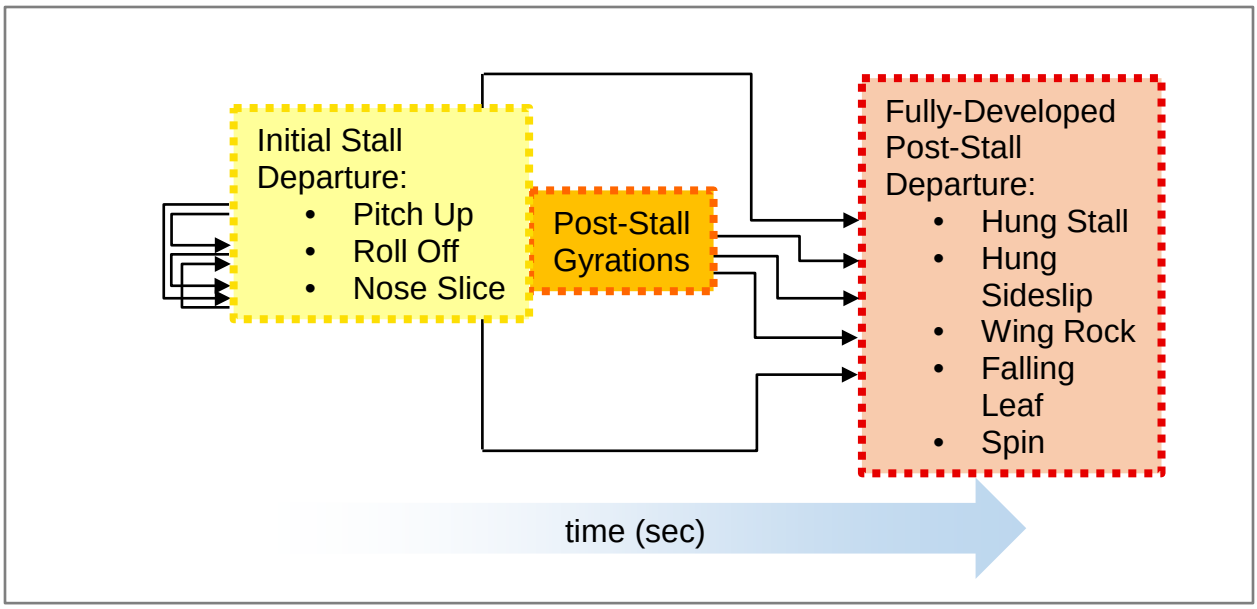

Figure 6. Schematic of the QSD definition process

In this top-level graphical representation, the identification/definition flow is represented by the arrows linking departure aspects in the three different phases. Each departure aspect is representative of a branch of the QSD definition logic tree in that phase. The process is shown looping back through specific stall-departure characteristics that are typically possible in the initial phase. As this time-stepping process unfolds, one or more initial-phase departure characteristic may be experienced in sequence. The QSD definitions method was designed to identify them and establish the time sequence between them in their initial-phase aspects. Beyond the initial phase, a different post-stall aspect of the same stall departure characteristic may be exhibited immediately after in the fully developed phase without passing through the post-stall-gyrations phase (e.g., a pitch-up transitioning into a hung stall or a nose-slice into a hung sideslip or a spin). There are other possible paths, with or without a transition through the post-stall-gyrations phase, as indicated by the results of the desktop and pilot-in-the-loop simulations study.

The QSD definitions developed in Task 1 for the different departure aspects in each of these phases were used sequentially along the time histories of each of the simulated stall maneuvers to identify the stall and post-stall departure aspects exhibited by the EURS.

Two of the most basic flight-test stall maneuvers are wings-level stalls and turning stalls with either a -1 or -3 knots-per-second entry rate. In these stall maneuvers, stall recovery is typically initiated following stall ID. In some cases, the column is pulled to the aft stop after stall ID and held momentarily before recovering. The more aggressive of these can reveal the stall characteristics in the initial phase of the departure. One such case is shown in figure 7, in which time histories for a wings-level stall on the left and a turning stall on the right are compared.

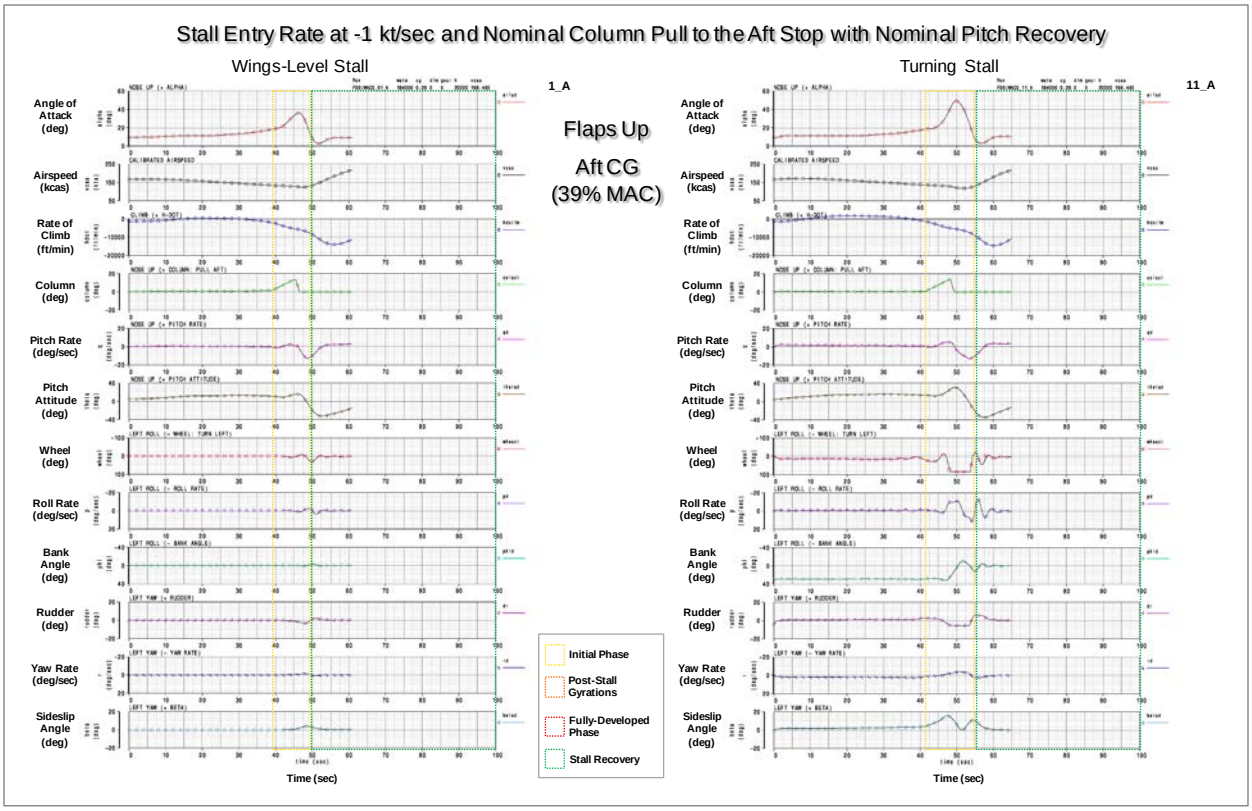

Figure 7. EURS stall departure in the initial phase of nominal stalls

The parameters in this selection of time-history plots provide essential information for identifying the type of stall and post-stall departures exhibited by the EURS model in these desktop stall simulations. The sign and direction-of-motion convention adopted for all time-history plots is that parameter traces trending towards the top of the plots denote nose-up motion for the pitch-axis parameters, and motion to the left for the roll- and yaw-axis parameters. There are five supplemental selections of parameters plotted in time-history format and two in cross-plot format. Related parameters were grouped to address particular aspects of the stall and post-stall defining motions. These other selections (plot templates) were used to more definitively identify a stall departure aspect and to further expand the defining parameter relationships conceptualized in Task 1.

These two stalls are representative of a lightweight, aft CG condition. At 39 seconds, stall ID (18º angle of attack), a nominal column pull to the aft stop drives angle of attack up to 36º in the wings-level stall and to 45º in the turning stall. A prompt, pitch-recovery column input to neutral with a nominal 1-second delay results in only a hint of post-stall lateral directional activity in the initial phase of the wings-level stall. Conversely, the turning stall, with a deeper penetration into the post-stall regime, exhibits a distinct left nose slice in the initial phase of the stall departure.

The nose slice is followed by a stabilizing roll off to the left, which counters the sideslip build-up from the nose slice. This is an example of two different stall departure aspects occurring sequentially in the initial phase and in which the second is in response to the first, but they can be

differentiated by the QSD sign relationships between roll rate, yaw rate, bank angle, and sideslip angle. Evident as well is the loss in lateral control above 30º angle of attack, approximately where a full right wheel applied by the roll math pilot is unable to counter the left roll and maintain the 30º bank angle to the right in the turning stall maneuver.

Figure 8 shows the same comparison of these two types of stall maneuvers at a faster entry rate, and with a 60-second delay in the pitch recovery maneuver. This delay revealed a well-defined, limit-cycle, oscillatory post-stall departure in the fully developed phase after transitioning from the same initial nose-slice/roll-off departure sequence observed in the nominal stall maneuvers (figure 7).

The higher post-stall angle of attack reached in the turning stall maneuver (plots on the right) is centered in a range of wing-rock susceptibility approximately between 30º and 60º angle of attack. In the wings-level stall, the post-stall angle of attack is approximately 10º lower with one excursion dipping below this susceptible range.

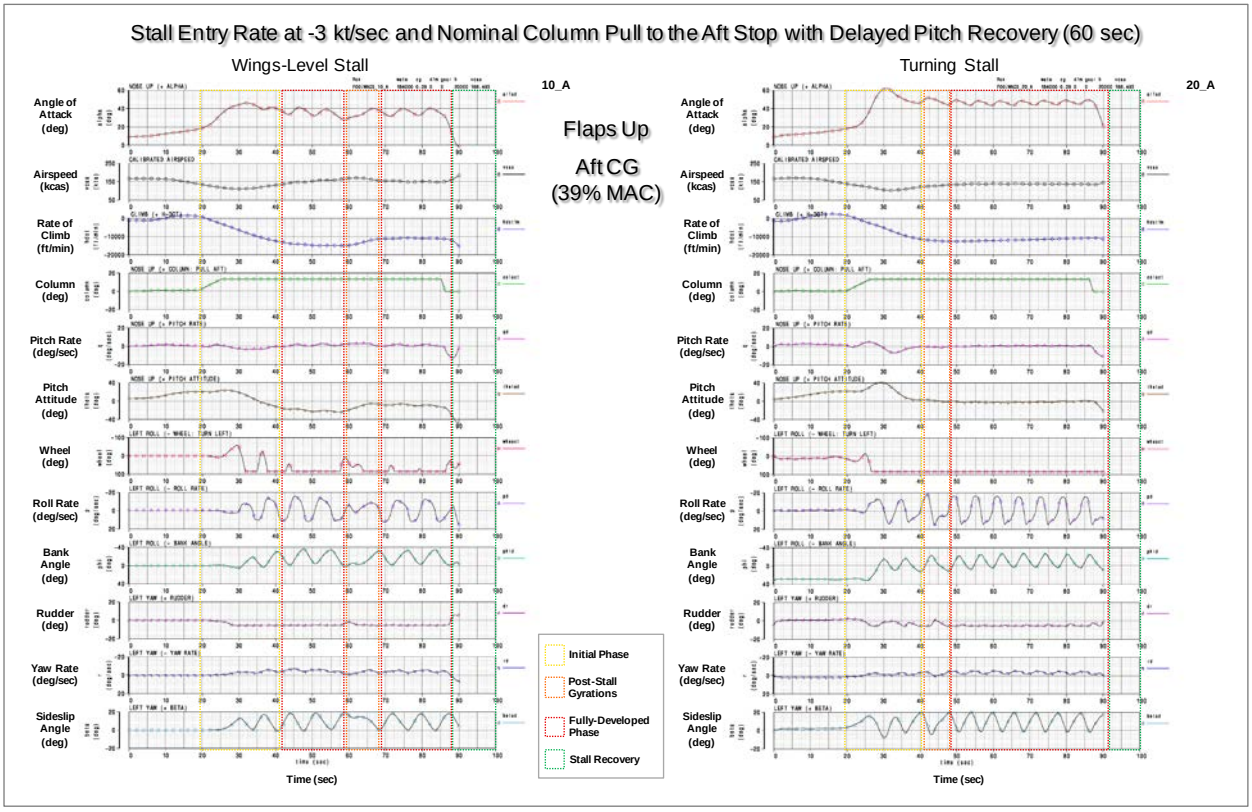

Figure 8. EURS fully developed post-stall departures at the aft CG limit

While this wing-rock departure characteristic is repeatable and well defined in both stall maneuvers, the frequency is higher for the turning stall, and there is a random break in wings-level stall when one of the post-stall oscillations in angle of attack dips below 30º after two full cycles of rolling motion.

Another less perceptible aspect in these fully developed post-stall departures is the slow spiral-like motion to the left, identified by the yaw rate and bank angle, both with mean values to the left. While not fitting most of the parameter relationships defining a fully developed spin, it does exhibit a constant rate of change in heading angle (not shown) giving rise to one spiral revolution in just more than a minute for the wings-level stall maneuver in which the post-stall departure rolls to a steeper, mean bank angle.

In figure 9, the same two commanded deep-stall maneuvers at the forward CG limit exhibit fully developed stall departures that are radically different from the limit-cycle, oscillatory departures observed at the aft CG limit in figure 8. Because of the increased longitudinal stability at the forward CG, the maximum angle of attack was approximately 10^{o} lower than in the stall maneuvers at the aft-CG-limit. The initial nose-slice departure is still present in both the wings-level and turning stall maneuvers at the forward CG. However, at this CG, the departure instead transitions into a steady, hung-sideslip departure in the fully developed phase.

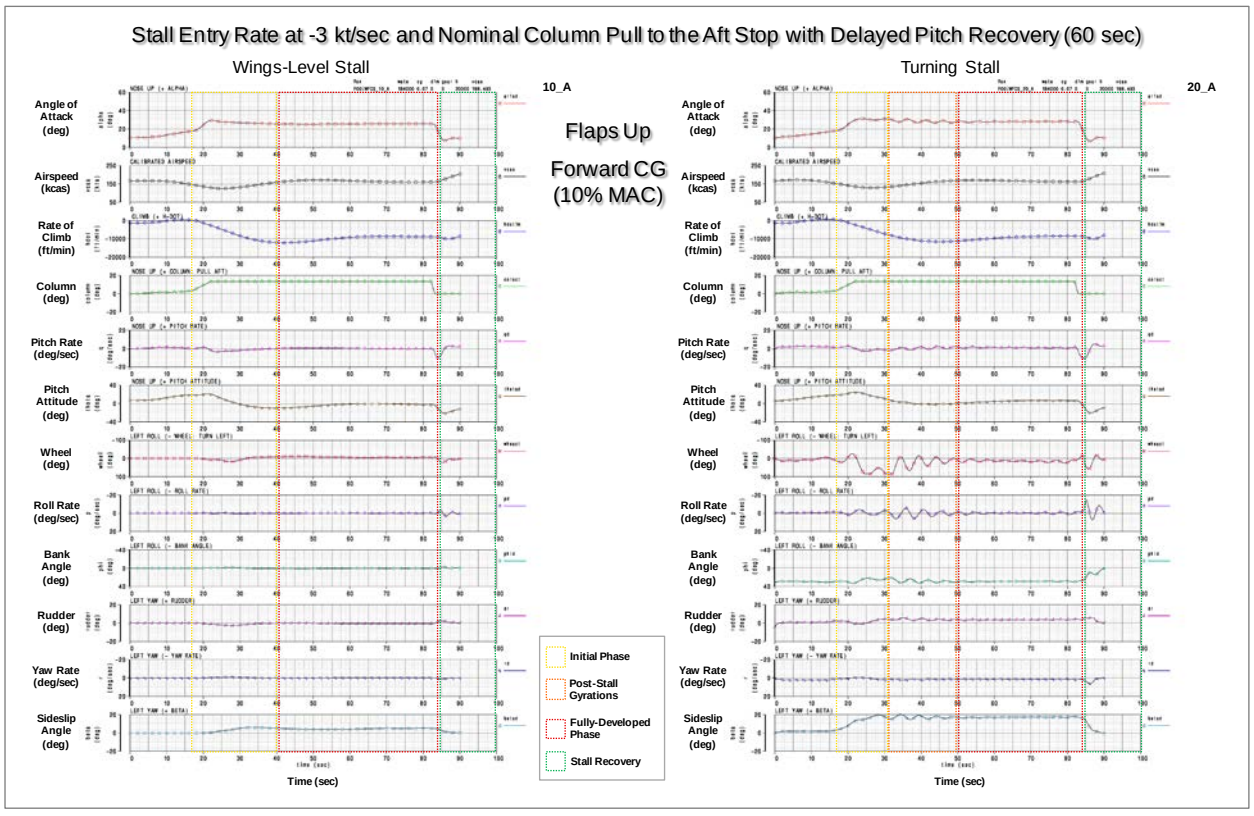

Figure 9. EURS fully developed post-stall departures at the forward CG limit

The larger sideslip angle in the hung-sideslip departure of the turning stall is due to the left-rudder deflection commanded by the yaw damper that compounds the adverse aerodynamic yaw-damping moment to the left. There is an oscillatory component classified as a post-stall gyration because it eventually dissipates and does not develop into any of the limit-cycle oscillatory departure aspects in the fully developed phase. This oscillatory component may be linked to the wing-rock susceptibility exhibited at the higher post-stall angles of attack reached at the aft CG limit. At the forward CG, the initial peak angle of attack may have just exceeded the lower bounds of the angle

of attack range of the wing-rock susceptibility. Again, recovery is immediate in this steady-state sideslip departure after angle of attack is driven below stall by moving the column to neutral during the recovery maneuver.

Figure 10 shows the effect of slowing the column pull to the aft stop for the same type of wings-level, commanded, deep-stall maneuvers shown in figure 8. The comparison between the time histories on the left and right shows the effects of shutting off the roll math pilot and yaw damper. Both maneuvers start to undergo roll and yaw excursions soon after the aft column input at stall ID begins and angle of attack starts increasing. However, once past the initial phase of the stall departure, these excursions differ in the post-stall randomness level that develops with time. The stall on the right was the baseline stall used in all stall maneuvers that explored the isolated effects of lateral/directional control step inputs of different duration. The different step inputs confirmed the typical decay in lateral/directional control effectiveness experienced through all phases of stall departure. Some level of rudder-control effectiveness was found to persist into the high post-stall angles of attack reached at the aft CG limit. No control reversals were detected.

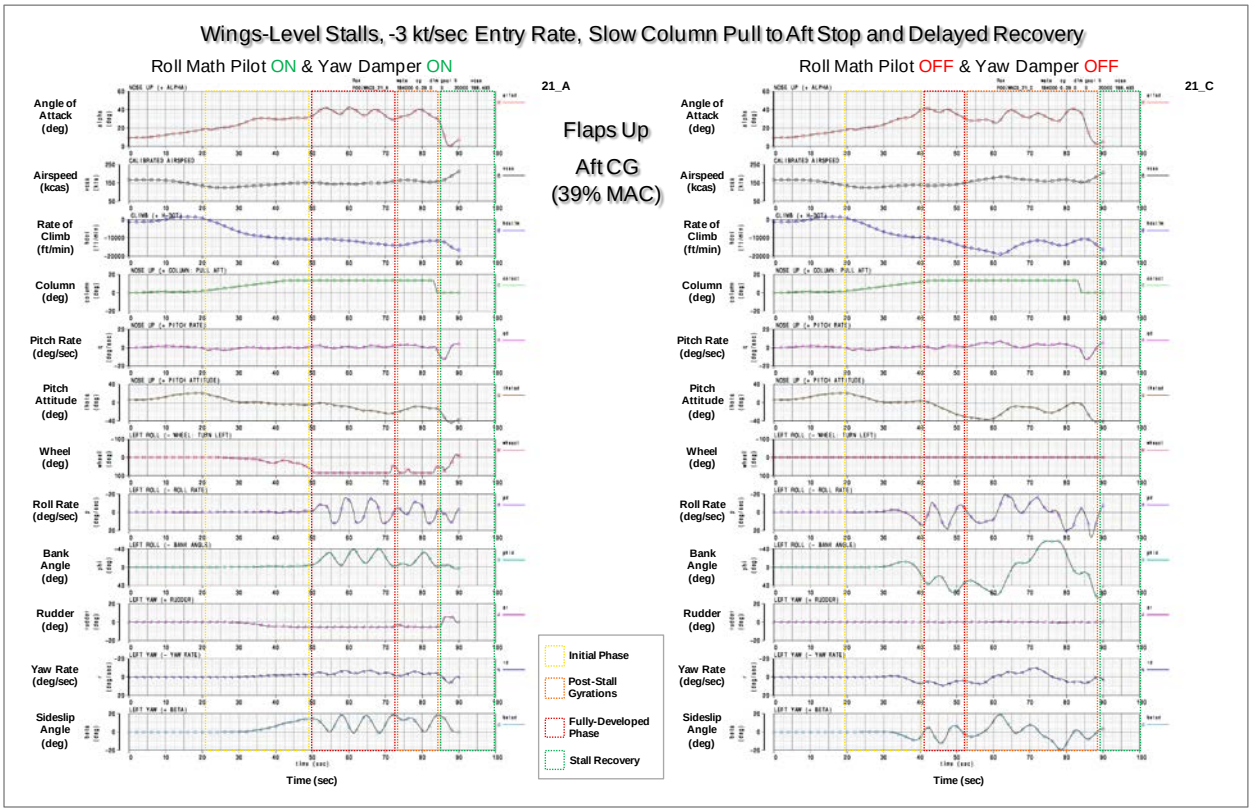

Figure 10. Effect of roll math pilot and yaw damper on EURS stall departure

In all the stall maneuvers studied, none of the lateral/directional control inputs, alone or in pro-spin combinations, led to a fully developed spin, as notionally defined in Task 1. However, because the rudder retains some of its control effectiveness, a slow spinlike departure was achieved, maintaining full rudder deflection after the initial stall phase.

Figure 11 shows two of these stall maneuvers in which the simulations were driven by rudder deflection, thus overriding systems in place that may limit rudder deflection at these conditions. The full right-rudder input resulted in a fully developed, oscillatory spiral to the right with a mean yaw rate that was approximately twice that with zero rudder deflection. The plots on the right show that a full recovery is achieved when both column and rudder are returned to neutral.

An attempt to recover in pitch alone with the column to neutral while holding full rudder failed, leading to a slightly higher spin rate and what appeared to be a hint of a falling-leaf departure developing with angle of attack swings between 10º and 50º, without any sign of a recovery in pitch. Another attempt at "breaking" the faster oscillatory spiral/spin by recovering with a full-forward column input resulted in a better defined falling-leaf departure as demonstrated by the plots on the right in figure 11.

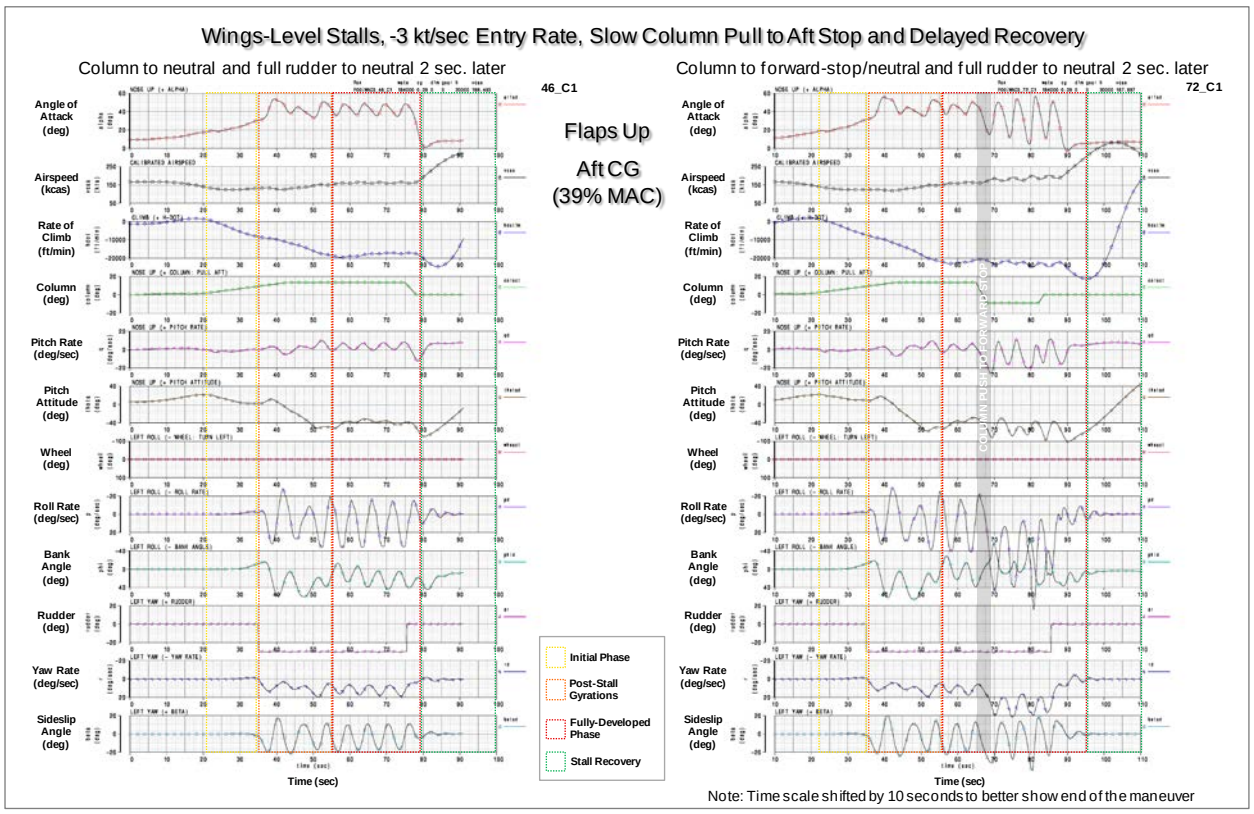

Figure 11. EURS slow oscillatory-spiral/spin and falling-leaf departure time histories

Pulling the column from full forward to neutral near the end of the time history did not have an effect on the character of the falling leaf. Only when the rudder was driven to neutral 2 seconds later was a recovery achieved, although at very high speed while pitching through over 120º from nearly straight down.

A review of companion time-history and cross plots in figure 12 highlights the differences between these two fully developed spinlike departures. The defining attributes of a spin that were developed in Task 1 (figure 3) are approximated here (e.g., a very steep flight-path angle nearly pointing down, a constant rate of change in heading angle, and near alignment of the velocity and rotational

vectors as calculated based on the mean values of roll and yaw rates). Both departures exhibited limit-cycle, oscillatory components.

However, a fully developed spinlike departure is denoted by parameter mean values being relatively steady. Both of these departures would better fit a slow, oscillatory spiral/spin definition because of the oscillatory nature of rotational responses and downward alignment of velocity vector being slightly off the vertical, resulting in a spin radius more representative of a spiral. This characterization was confirmed by pilot comments during the pilot-in-the-loop assessment. The falling-leaf departure was more spinlike with a turn rate that was more than three times as fast with a slightly tighter spin radius at a 5º steeper mean flight-path angle. Besides the difference in spin rate between the slow, oscillatory spiral/spin and the falling leaf, the definitive discriminator between these two post-stall departure aspects is the nature of the oscillatory components in the angle-of-attack and sideslip excursions.

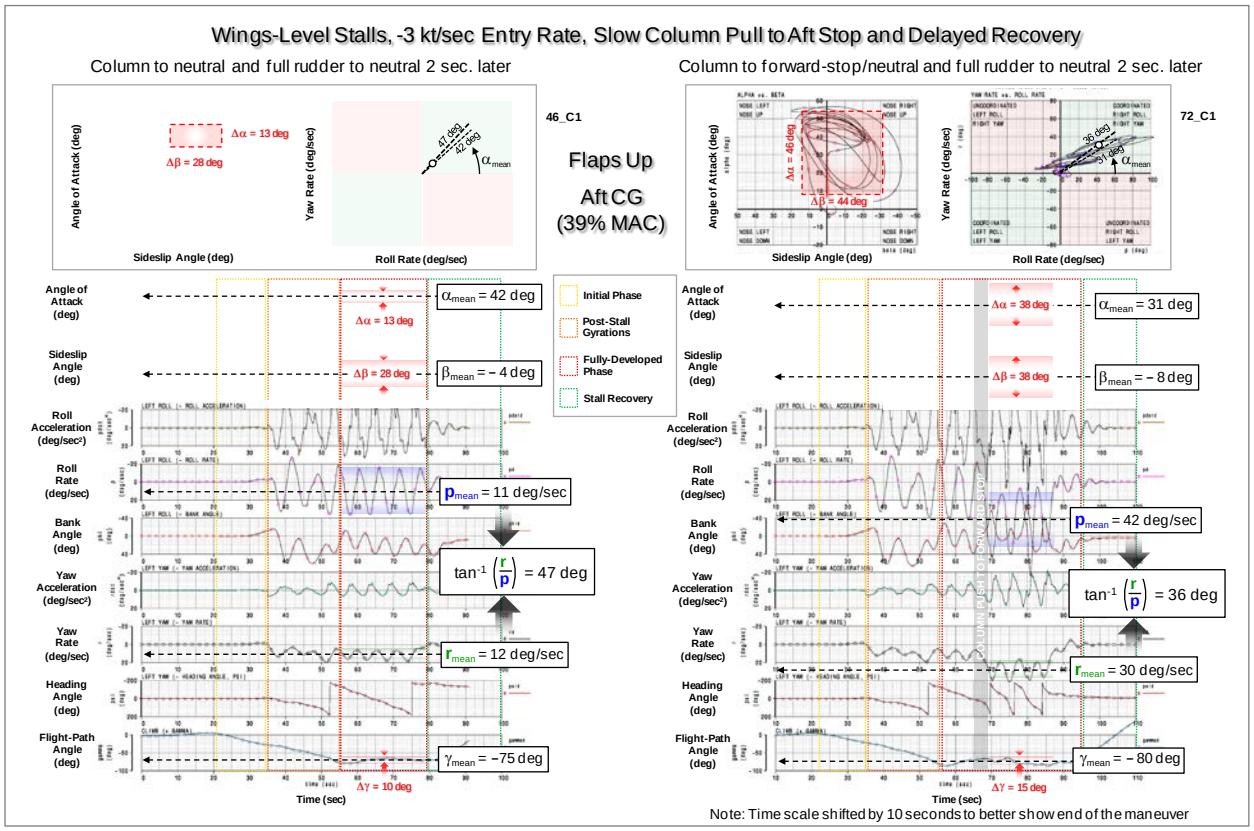

Figure 12. EURS slow oscillatory-spiral/spin and falling-leaf departure time histories and cross-plots

A comparison between the angle-of-attack and sideslip cross plots in figure 12 highlights the different shape of the oscillatory simulation traces and the different ratio of angle-of-attack and sideslip amplitude between the two departures. In the cross plot on the right, one can clearly see the transition between these two departure aspects in the same stall maneuver.

The desktop simulation assessment revealed that the EURS exhibits several different aspects of yaw and roll departures at the light weight and extreme CG conditions investigated. Most of these

were present only during commanded deep-stall maneuvers in which the column was held at the aft stop for up to a minute, allowing the stall departure to fully develop. Some of these departure aspects were the result of aggressive post-stall control inputs seldom observed in large transport outside of accident scenarios.

The pilot-in-the-loop simulation assessment that followed was aimed at confirming these different departure aspects and searching for any that may have been missed in the desktop assessment. For example, none of the combinations of lateral and directional control inputs in the commanded deep-stall maneuvers revealed a controls-neutral spin departure. Pilot impressions were also sought to solidify the defining attributes in the QSD process.

Figure 13 shows a snapshot of a composite display during a pilot-in-the-loop simulation of the slow, oscillatory spiral/spin departure in the fully developed phase.

Figure 13. Pilot-in-the-loop simulations in multipurpose cab (M-Cab) at Boeing

All simulations were flown by experienced Boeing test pilots familiar with the stall characteristics of the type of large transport airplane that the EURS model is intended to simulate. Adherence to dispatch requirements was recognized by having the yaw damper active at all times. The rudder ratio changer, which was disabled in some of the desktop simulations, was active as well.

Figure 14 captures the vastly different stall-departure characteristics at the forward and aft CG limits in two different stall maneuvers confirming findings in the desktop assessment. The time-history plots on the left for the turning stall at the forward CG limit shows a nose-slice departure

transitioning into a fully developed hung-sideslip departure. This departure with the pilot controlling bank angle was much steadier than the companion desktop simulation example in figure 9, in which the roll math pilot activity may have contributed to the initial oscillatory character of essentially the same post-stall departure.

The slight difference in CG (7% vs. 10% MAC in the desktop example) may have also contributed to the oscillatory character in the desktop simulation maneuver in which the angle-of-attack excursion initially penetrates the lower threshold of the wing-rock susceptible range.

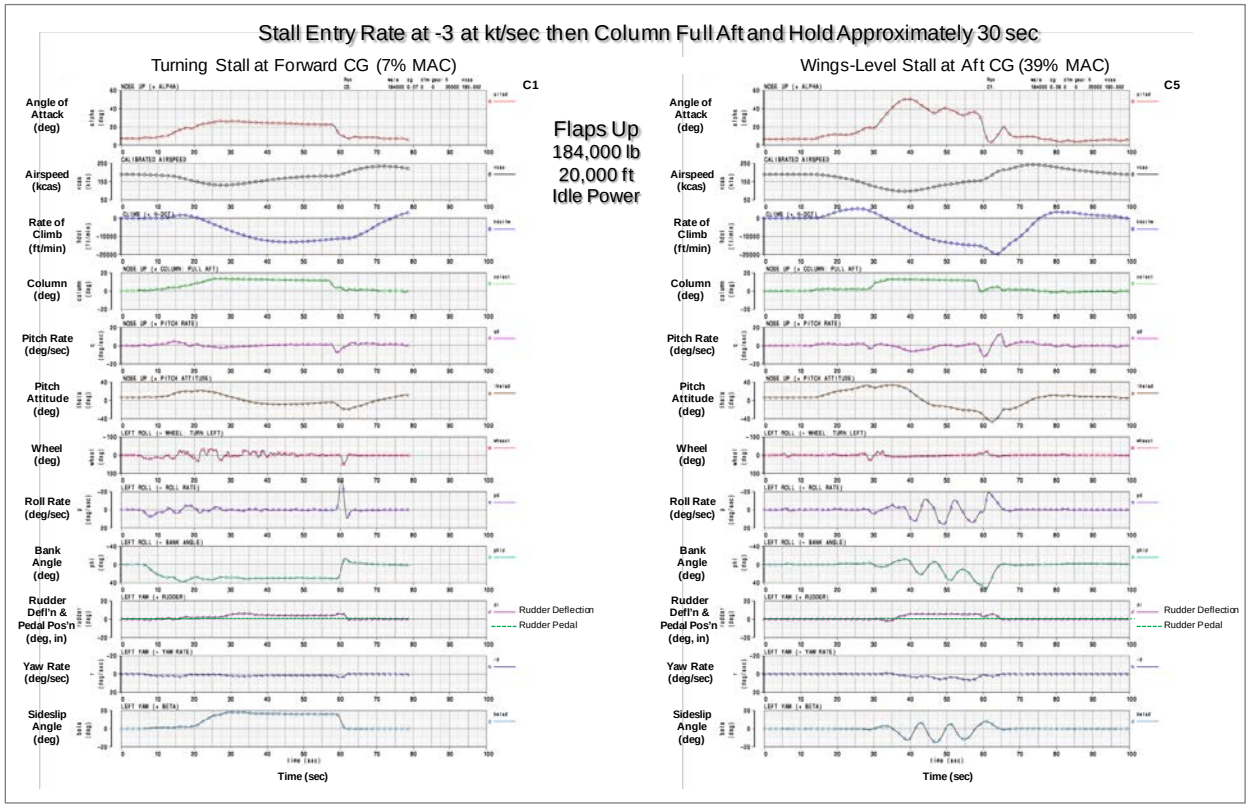

Figure 14. EURS stall departures at the forward and aft CG limits in pilot-in-the-loop simulations

The time history plots on the right confirm this lower threshold at an approximate 30º angle of attack in which the wing-rock departure fully develops into the same type of slow spiral departure observed in desktop simulations at the aft CG limit (figure 8). As shown in figure 14, the initial stall departure may have been induced by the pilot attempting to correct the bank-angle build-up to the left during the stall approach. The right-wheel pulse at 28 seconds precedes the roll rate to the right and sideslip to the left as specified by the QSD roll-rate/sideslip relationship in a roll-off departure. A secondary nose-slice departure followed as yaw rate and sideslip to the left increased before transitioning into the wing-rock departure in a slow spiral departure lasting approximately 15 seconds, before a full recovery was achieved.

The effect of more aggressive lateral and directional control inputs was explored as part of the pilot-in-the-loop assessment. The decay and loss of lateral control was confirmed and considered

adequately modeled. Rudder inputs of various magnitudes and durations confirmed the decay in rudder effectiveness. Attempts to maintain bank angle with rudder through the stall and stall-recovery maneuvers were explored. This task proved difficult as a result of lag in the roll response and interference from the yaw damper. The pilots searched for a better defined spin departure with rudder alone and pro-spin wheel and rudder control inputs at mid- and aft-CG locations, and at idle- and FAR-power settings. All attempts, including an extremely dynamic stall maneuver with angle of attack peaking at 70º, failed to produce a fully developed spin departure.

Aggressive use of the rudder and column inputs by the pilots were required to replicate the most complex post-stall departure demonstrated in the desktop simulations: the slow oscillatory spiral/spin at the aft CG limit, the transition to a falling leaf induced by a column push from the aft stop to the forward stop, and the full recovery from this violent departure by driving all controls to neutral.

Figure 15 shows an example of such a maneuver, which approximates the character of the same type of maneuver in the desktop simulation example in figure 14. This is a more realistic stall maneuver in which the yaw damper is active, and the pilot attempts to maintain wings level after the first and only violent cycle of the falling-leaf departure in which the kinematic coupling of a sharp left roll drives angle of attack down from approximately 50º to slightly negative, whereas sideslip increases to the right at a nearly 1:1 ratio.

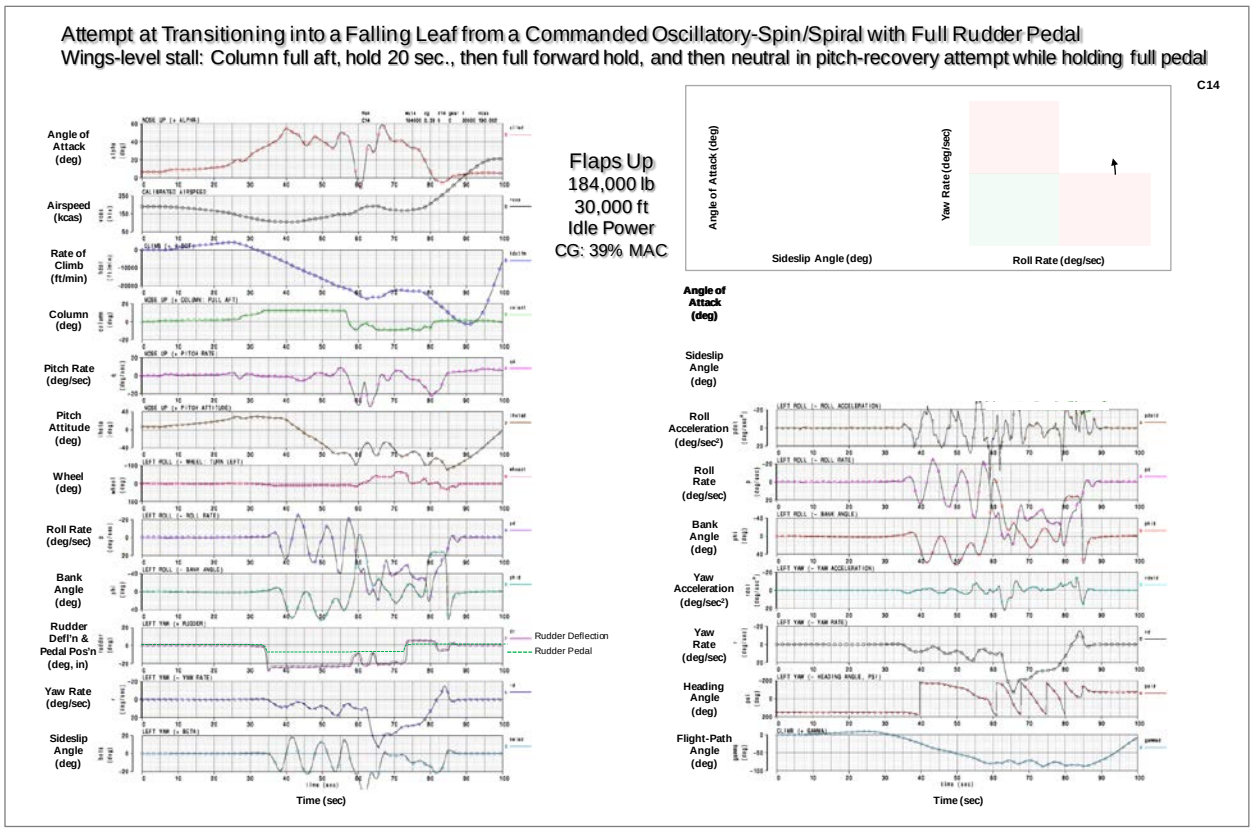

Figure 15. EURS slow oscillatory-spiral/spin and falling-leaf departures in a pilot-in-the-loop simulation

On the cross plot of angle of attack and sideslip, these variations can be recognized as one loop/cycle of the characteristic mushroom-shape trace of a falling-leaf departure, as described in the literature [6], in which angle of attack swings from high to low as sideslip swings opposite from low to high. The correcting wheel input, and possibly the yaw-damper activity, may have prevented the additional open-loop cycles of the falling leaf present in the open-loop (i.e., both roll math pilot and yaw damper off) desktop simulation.

In summary, the stall and post-stall departure characteristics identified in the desktop simulation assessment were confirmed by pilot-in-the-loop simulations. Results from these two simulation assessments indicate that the EURS does exhibit stall characteristics that are representative of this type of transport airplane in the initial phase of the stall departure. In the fully developed phase, the post-stall departure characteristics, and all their different aspects, could not be confirmed as representative because of lack of flight data and experience in this flight regime commanding and holding aggravating control inputs.

The overall assessment of the EURS simulation by the Boeing test pilots is that although it does exhibit these departure characteristics, it was their professional opinion that the post-stall aerodynamics modeling was “too benign, too stable,” considering the aggressive control inputs, particularly rudder, required to excite some of the post-stall departure aspects encountered. However, the rotation rates and accelerations, and consequent structural demands on some of the airplane components, were not deemed benign at all. In fact, the high speeds and excessive normal and lateral load factor values registered, which would most likely compromise the structural integrity of the airplane, should be considered when assessing the realism of these stall departures and recoveries. It is possible that the inherent stability of conventional large-transport airplanes, such as that modeled by the EURS (i.e., as captured by the post-stall, wind-tunnel-based model aerodynamics) indeed results in benign and fully recoverable post-stall departures.

Another observation was that the modeling of “lateral instabilities” in the stall onset prior to the initial phase of the stall departure lacked realism, requiring little or no pilot workload to maintain wings-level or bank angle in a turning stall. The perceived “instabilities” were mild and occurred late in the stall maneuver, which suggests an earlier start at a lower angle of attack would improve simulation fidelity.

Some of the pilot comments regarding the absence of a fully developed spin can be the result of the absence of a steady-state rotational model based on rotary-balance wind-tunnel data, which enhances the fidelity of spin aerodynamics modeling.

These observations were all tempered by the pilots asserting that their opinions were based on their experiences with less stable, non-transport type airplanes as well as with large transport-type airplanes, with occasional penetrations into the post-stall regime during stall characteristics certification testing of the latter. However, none of these penetrations were conducted with aggravated control inputs similar to those in these simulations.

3. SUMMARY OF PHASE 2

Phase 1 of this project focused on the development of quantitative definition of stall departure in all its manifestations and individual aspects, and in identifying, through these definitions, which

of these were exhibited in desktop and pilot-in-the-loop stall simulations with the EURS aerodynamics model.

Task 1 of Phase 2 focused on which components/parameters in the EURS model were primarily associated with the stall and post-stall departure characteristics identified in Phase 1. It also explored the level of accuracy and range required when modeling these components/parameters for a similarly configured transport airplane as that modeled by the EURS. These results were then used in Task 2 to determine the level of effort required to develop such a model, and the total cost of the effort associated with analysis and/or wind tunnel testing.

3.1 CORRELATION OF EURS MODEL PARAMETERS WITH STALL DEPARTURE ASPECTS

Several individual aspects of the EURS stall and post-stall departure characteristics were identified in desktop simulations by applying the QSD definitions developed in Phase 1. These individual departure aspects are listed below in the combinations and sequence in which they were identified in several aggravated stall maneuvers:

1. Initial stall-phase nose-slice followed by stabilizing roll off
2. Initial stall phase coordinated roll-off followed by opposite nose slice
3. Fully developed, post-stall phase, “hung” sideslip
4. Fully developed, post-stall phase, wing-rock in a slow, oscillatory spiral
5. Post-stall wing-rock followed by post-stall gyrations never developing fully into a slow oscillatory spiral (roll math pilot OFF and yaw damper OFF)
6. Decay of lateral and directional control effectiveness
7. Commanded slow, oscillatory spiral/spin (full rudder hold)
8. Commanded falling leaf (full forward column with full rudder)

Certification requirements ensure benign and controllable stall characteristics up to stall ID and through the recovery. Most of these stall-departure aspects, particularly those in their fully developed form, were the result of aggravating control inputs, some held as long as 60 seconds, driving the simulation far beyond the typically benign stall characteristics exhibited in nominal flight-test stall maneuvers in which recovery is prompt and uneventful. While stall-characteristics flight testing is an important component of airplane certification, instances of stall departure are rare in transport-category airplanes because they are designed to be inherently stable. Shallow penetrations into the post-stall regime occur occasionally while establishing certifiable stall-recognition characteristics, but these never result in severe departures. Only intentional control inputs or a significant yaw asymmetry, such as an engine out, would cause the more severe stall departure aspects listed above.

Taking all this into consideration, it is not certain that the post-stall aerodynamics modeled by the EURS represent those of a full-scale, certified airplane configuration. It then follows that some of the deep-stall departure aspects identified in these simulations may not be exhibited by this airplane in full-scale flight stalls.

More than 200 flaps-up stall maneuvers were analyzed in the desktop simulation assessment in Task 2 of Phase 1. Fifteen of these stall maneuvers were selected to develop a correlation matrix

linking each individual parameter in the EURS aerodynamics model to the individual EURS stall-departure aspects identified. Figure 16 describes these 15 stall maneuvers and the stall departure aspects identified in the different stall departure phases of each. They were selected because, as a group, these stall maneuvers exhibited all the stall-departure aspects identified. Each of these stall maneuvers exhibited one or more of these departure aspects and were appropriately grouped to explore the impact of each EURS model component/parameter on the simulation fidelity of each individual departure aspect.

Figure 16. Selection of stalls for EURS Model Parameter Correlation Study

In this context, a model component/parameter refers to a single force or moment parameter associated with a major component in the EURS aerodynamics model. For example, EURS rudder effectiveness is a major component of the model with the yawing moment due to rudder deflection being a parameter of this major component. Each EURS parameter is the sum of the corresponding baseline parameter (i.e., a parameter which may comprise a single or several related tables in the underlying non-EURS baseline model) and an incremental ΔEURS parameter, modeled as a single table, which when added to the baseline parameter incorporates the EURS stall and post-stall characteristics. This sum essentially extends the post-stall range of the baseline parameter with accurate data from dedicated EURS static and dynamic tests.

Figure 17 illustrates the build-up of the parameter for the basic tail-on, flaps up, directional static stability of the EURS model. In the non-EURS model, this parameter is the sum of two tables: the contribution of the wing-body, or tail-off component (fuselage with the horizontal tail, wing and engine nacelles) and that of the vertical tail. The corresponding EURS model parameter is a tail-on parameter, modeled as an incremental effect table, added to the sum of the two non-EURS model tables. In essence, this incremental ΔEURS table adjusts the sum of the two non-EURS

tables, such that the total of these three tables exhibits the stall and post-stall aerodynamic characteristics as determined from wind-tunnel tail-on test data of the twin-jet transport configuration modeled by the EURS.

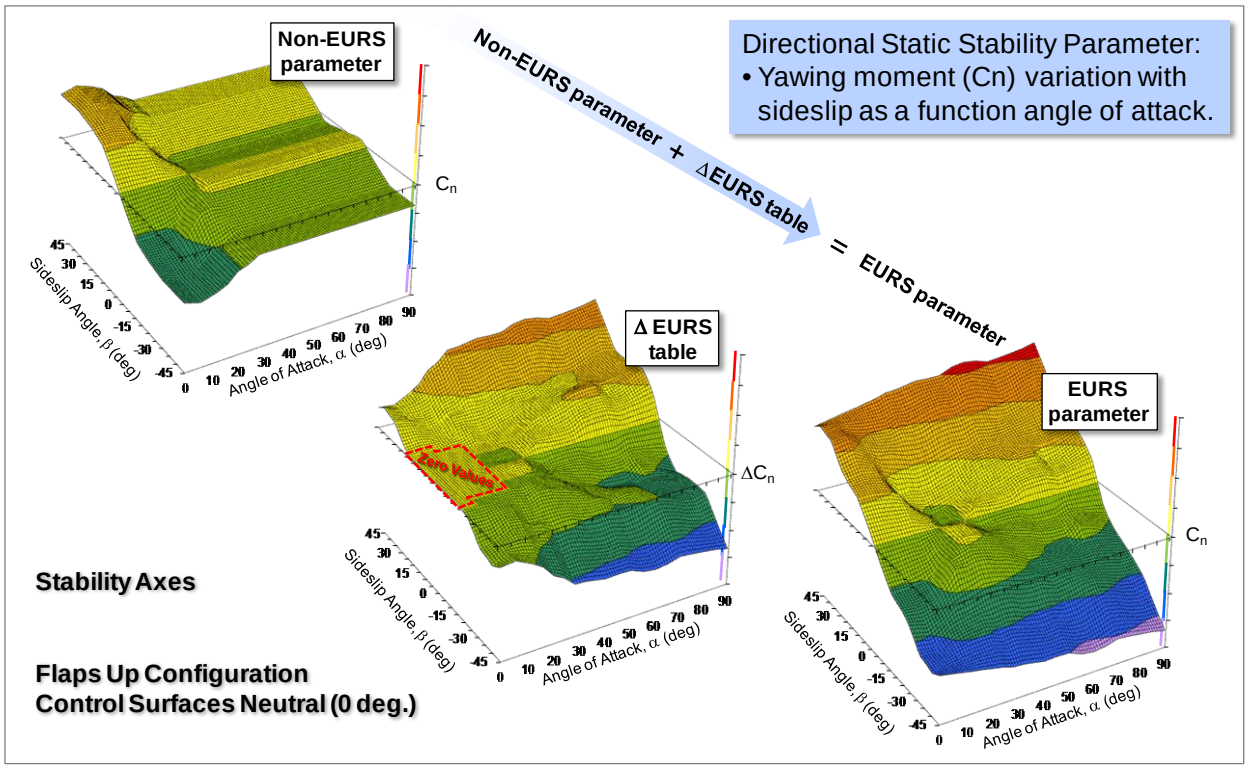

Figure 17. EURS parameter buildup from the corresponding non-EURS parameter

The ΔEURS table (center) has zero value between ±20 degrees of sideslip at the lower angles of attack and ±15 degrees sideslip on approach to stall through 20º angle of attack (red-dashed region). The non-zero values in this table correct the hold-last-value-constant extrapolations of the underlying non-EURS baseline model parameter (top left) by introducing accurate stall and post-stall values, as modeled by the parameter sum (bottom right). Zeroing out the entire EURS increment table effectively returns the EURS model values of this parameter to those of the underlying non-EURS baseline model. A simulation of one of the selected stall maneuvers with this table zeroed out would show the effect of the EURS directional static stability parameter on the stall-departure aspects exhibited by the baseline EURS simulation. Two more parameters, rolling moment and side force due to sideslip, comprise the lateral/directional static stability component or parameter/table group. There were 40 such tables divided among 11 major model components, each having between 3 and 6 tables.

Figure 18 lists all 40 ΔEURS tables associated with the corresponding EURS and underlying baseline non-EURS model parameter. These 40 tables/parameters are divided into 11 groups aligned with major components of both the EURS model and the underlying non-EURS baseline model.

Table	Table Group	Table Group Definition	Table Name	Table Definition
1	# 1 longit_o_	Basic longitudinal forces, static stability and stabilizer effectiveness	eurdcdh	EURS basic tail-on drag, and stabilizer control effectiveness drag increment
2			eurdclh	EURS basic tail-on lift, and stabilizer control effectiveness lift increment
3			eurdcmh	EURS basic tail-on pitching moment, and stabilizer control effectiveness pitch increment
4	# 2 longit_b_	Incremental sideslip effects on basic longitudinal forces and static stability	eurdcdb	EURS the basic tail-on drag increment due to sideslip
5			eurdclb	EURS the basic tail-on lift increment due to sideslip
6			eurdcmb	EURS the basic tail-on pitch increment due to sideslip
7	# 3 latdir_b_	Basic tail-on lateral/directional static stability and side force	eurdcnb	EURS basic tail-on yaw due to sideslip
8			eurdcrb	EURS basic tail-on roll due to sideslip
9			eurdcyb	EURS basic tail-on side force due to sideslip
10	# 4 asymmetry	Incremental stall assymetries in roll, yaw and side force	eurcnasy	EURS effect/correction stall-asymmetry yaw increment with ± sideslip (same magnitude, but opposite sign)
11			eurcrasy	EURS effect/correction stall-asymmetry roll increment with ± sideslip (same magnitude, but opposite sign)
12			eurcyasy	EURS effect/correction stall-asymmetry side-force increment with ± sideslip (same magnitude, but opposite
13	# 5 elevator_	Elevator control effectiveness increments	eurdcde	EURS the elevator control effectiveness drag increment
14			eurdcle	EURS the elevator control effectiveness lift increment
15			eurdcme	EURS the elevator control effectiveness pitch increment
16	# 6 ailerons_	Aileron control effectiveness increments	eurdcna	EURS the aileron control effectiveness yaw increment
17			eurdcra	EURS the aileron control effectiveness roll increment
18			eurdcda	EURS the aileron control effectiveness drag increment
19			eurdcla	EURS the aileron control effectiveness lift increment
20			eurdcma	EURS the aileron control effectiveness pitch increment
21	# 7 spoilers_	Spoiler control effectiveness increments	eurdcnsp	EURS spoiler control effectiveness yaw increment blended via alpha/beta blending function (eursp)
22			eurdcrsp	EURS spoiler control effectiveness roll increment blended via alpha/beta blending function (eursp)
23			eurdcysp	EURS spoiler control effectiveness side-force increment blended via alpha/beta blending function (eursp)
24			eurdcdsp	EURS spoiler control effectiveness drag increment blended via alpha/beta blending function (eursp)
25			eurdclsp	EURS spoiler control effectiveness lift increment blended via alpha/beta blending function (eursp)
26			eurdcmsp	EURS spoiler control effectiveness pitch increment blended via alpha/beta blending function (eursp)
27	# 8 rudder__	Rudder control effectiveness increments	eurdcnr	EURS the rudder control effectiveness yaw increment
28			eurdcrr	EURS the rudder control effectiveness roll increment
29			eurdcyr	EURS the rudder control effectiveness side-force increment
30			eurdcdr	EURS the rudder control effectiveness drag increment
31			eurdcmr	EURS the rudder control effectiveness pitch increment
32	# 9 dyn_pitch	Incremental dynamic effect due to pitch rate	eurcddyn	EURS the dynamic increment of drag due to pitch rate
33			eurcldyn	EURS the dynamic increment of lift due to pitch rate
34			eurcmdyn	EURS the dynamic increment of pitch due to pitch rate
35	# 10 dyn_roll_	Incremental dynamic effect due to roll rate	eurcnpbh	EURS the dynamic increment of yaw due to roll rate
36			eurcrpbh	EURS the dynamic increment of roll due to roll rate
37			eurcypbh	EURS the dynamic increment of side force due to roll rate
38	# 11 dyn_yaw_	Incremental dynamic effect due to yaw rate	eurcnrbh	EURS the dynamic increment of yaw due to yaw rate
39			eurcrrbh	EURS the dynamic increment of roll due to yaw rate
40			eurcyrbh	EURS the dynamic increment of side force due to yaw rate

Figure 18. Definition of 40-parameter (ΔEURS tables) and 11-parameter groups associated with major EURS model components

These 40 tables were combined into 44 table-group combinations between 1 and all tables within each component group of parameters. As the correlation study progressed, the number of combinations were expanded to 48.

Figure 19 shows the 44 initial table combinations. Desktop simulations of the most appropriate stall maneuvers from the 15 identified for this study were run with each of the above combinations. The first combination with all 40 EURS increment tables zeroed out represented the non-EURS baseline model.

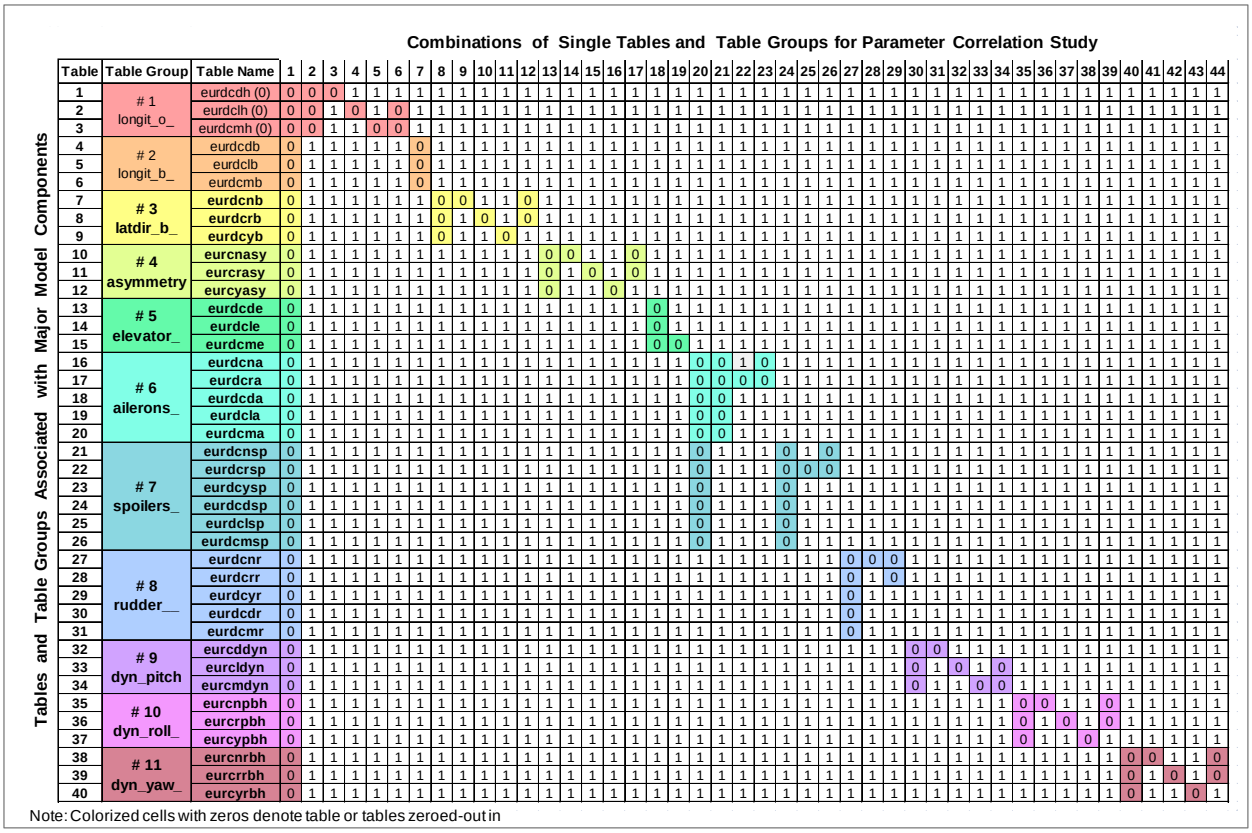

Figure 19. Table-group combinations for EURS Model Parameter Correlation Study

All 15 stall maneuvers were run to generate the worst-case baseline simulation responses for this study. A total of 150 stall/table-group combinations was investigated and more than 1800 plots were generated. A significant number of these plots was reviewed to determine the effect of each individual parameter on the EURS stall-departure aspects and the synergies among parameters within their respective group. These plots were the means of visualizing, in time-history and cross-plot formats, the pertinent basic flight parameters and derived parameters related to the QSD definitions of the departure aspects. The visual-inspection process relating deviations in the simulated responses between the zeroed-out-table cases and the baseline EURS was at the heart of the effort to correlate the EURS parameters to their impact on the individual stall-departure aspects. The following is a summary of the visual inspection results:

- In the Basic Longitudinal Statics table group, the pitching moment parameter had the most significant effect because it completely changed post-stall departure aspects by dramatically changing the maximum angle of attack of the departure.
- For the Basic Lateral/Directional Statics table group, stall characteristics were dependent on CG with simulations at the aft CG limit most affected. The forward CG was unaffected as the maximum angle of attack was below the threshold where the EURS aerodynamic characteristics are introduced. At the aft CG limit, oscillatory post-stall departure aspects were affected most in their frequency and amplitude, along with some phase shifts and mean-value biases.

- In the Elevator Control Effectiveness table group, the pitch parameter had a significant effect by changing the baseline EURS fully developed wing-rock departure to a hung-sideslip by reducing the maximum angle of attack of the post-stall departure.
- In the Lateral Control Effectiveness table group, full-wheel pulses at 24º and 39º angle of attack show that both rolling- and yawing-moment parameters significantly affected stall-departure aspects. The wheel input at the initial stall point (pulse at 24 degrees) had the greatest effect. A significant change in bank angle response resulted along with a change in the angle-of-attack response and the character of the post-stall wing-rock oscillations
- In the Rudder Control Effectiveness table group, the rudder yawing moment parameter had a significant effect on stall maneuvers with full-rudder inputs. Higher yaw rates and post-stall angles of attack were reached with the oscillatory character of the slow spiral/spin almost absent and the falling leaf failing to develop.
- In the 'Rate Damping Dynamics' table group, zeroing out the roll-damping parameter had the most noticeable effect on the EURS stall departure, particularly the post-stall wing-rock aspect in all aft-CG stall maneuvers.

Visual inspection of the stall time-history/cross plots provided the material for the development of the correlation matrix relating the power of each individual simulation parameter to affect the various individual aspects of stall departure, as summarized in figure 20. This matrix lists all 40 individual EURS model parameters/tables in rows on the left, as previously done in the table/table-group combination matrix in figure 19. In the remaining columns across the top are the 8 combinations of the individual stall and post-stall departure aspects of the EURS. Note that many of these aspects are found in several of the 15 stall maneuvers selected for this study. Some aspects, such as those related to specific lateral and directional control inputs, are applicable only in dedicated stall maneuvers #9 to #15.

			Combinations of Individual Aspects of EURS Stall and Post-Stall Departure Characteristics							
			Initial Stall: Nose-Slice	Initial Stall: Roll-off followed by oposite nose-slice ‡	Post-Stall: "hung" sideslip following nose-slice	Post-Stall: Wing-rock in slow oscillatory spiral	Post-Stall: Wing-rock followed by post-stall	Decay/Loss of lateral and directional control	Commanded slow, oscillatory spiral/spin: full	Commanded falling leaf: full forward column with full
Table	Table Group	Table Name	1	2	3	4	5	6	7	8
1	# 1 longit_o_	eurdcdh (0)	Minor effect	No effect *	No effect *	Minor effect	Minor effect *	Not Applicable	Minor effect *	Minor effect *
2		eurdclh (0)	No effect	No effect *	No effect *	No effect	No effect *	Not Applicable	No effect *	No effect *
3		eurdcmh (0)	Significant effect	Significant effect *	Minor effect *	Significant effect	Significant effect *	Not Applicable	Significant effect *	Significant effect *
4	# 2 longit_b_	eurdcdb	No effect *	No effect *	No effect *	No effect *	No effect *	Not Applicable	No effect *	No effect *
5		eurdclb	No effect *	No effect *	No effect *	No effect *	No effect *	Not Applicable	No effect *	No effect *
6		eurdcmb	Minor effect	Minor effect *	No effect *	Minor effect	Noticeable effect	Not Applicable	Minor effect *	Minor effect *
7	# 3 latdir_b_	eurdcnb	Minor effect	Minor effect *	No effect	Minor effect	Minor effect *	Not Applicable	Significant effect	Significant effect
8		eurdcrb	Minor effect	Minor effect *	No effect	Significant effect	Significant effect *	Not Applicable	Noticeable effect	Noticeable effect
9		eurdcyb	No effect	No effect *	No effect	No effect	No effect *	Not Applicable		
10	# 4 asymmetry	eurcnasy	Minor effect	Minor effect *	No effect	Minor effect	Minor effect *	Not Applicable	Minor effect *	Minor effect *
11		eurcrasy	Minor effect	Minor effect *	No effect	Noticeable effect	Noticeable effect *	Not Applicable	Minor effect *	Minor effect *
12		eurcyasy	No effect	No effect *	No effect	No effect	No effect *	Not Applicable	No effect *	No effect *
13	# 5 elevator_	eurdcde	No effect	No effect *	No effect *	No effect	No effect *	Not Applicable	No effect *	No effect *
14		eurdcle	No effect	No effect *	No effect *	No effect	No effect *	Not Applicable	No effect *	No effect *
15		eurdcme	No effect	Significant effect *	Noticeable effect *	Significant effect	Significant effect *	Not Applicable	Significant effect *	Significant effect *
16	# 6 ailerons_	eurdcna	Not Applicable	Noticeable effect ‡	Not Applicable	Noticeable effect *	Noticeable effect	Noticeable effect	Not Applicable	Not Applicable
17		eurdcra	Not Applicable	Significant effect ‡	Not Applicable	Noticeable effect *	Noticeable effect	Significant effect	Not Applicable	Not Applicable
18		eurdcda	Not Applicable	No effect ‡ *	Not Applicable	No effect *	No effect *	No effect *	Not Applicable	Not Applicable
19		eurdcla	Not Applicable	No effect ‡ *	Not Applicable	No effect *	No effect *	No effect *	Not Applicable	Not Applicable
20		eurdcma	Not Applicable	Minor effect ‡ *	Not Applicable	Minor effect *	Minor effect *	Minor effect *	Not Applicable	Not Applicable
21	# 7 spoilers_	eurdcnsp	Not Applicable	Noticeable effect ‡	Not Applicable	Noticeable effect *	Noticeable effect *	Noticeable effect *	Not Applicable	Not Applicable
22		eurdcrsp	Not Applicable	Significant effect ‡	Not Applicable	Noticeable effect *	Noticeable effect *	Significant effect *	Not Applicable	Not Applicable
23		eurdcysp	Not Applicable	No effect ‡ *	Not Applicable	No effect *	No effect *	No effect *	Not Applicable	Not Applicable
24		eurdcdsp	Not Applicable	No effect ‡ *	Not Applicable	No effect *	No effect *	No effect *	Not Applicable	Not Applicable
25		eurdclsp	Not Applicable	No effect ‡ *	Not Applicable	No effect *	No effect *	No effect *	Not Applicable	Not Applicable
26		eurdcmsp	Not Applicable	Minor effect ‡ *	Not Applicable	Minor effect *	Minor effect *	Minor effect *	Not Applicable	Not Applicable
27	# 8 rudder__	eurdcnr	Not Applicable	Significant effect	Not Applicable	Significant effect	Significant effect *	Significant effect	Significant effect	Significant effect
28		eurdcrr	Not Applicable	Minor effect	Not Applicable	Minor effect	Minor effect *	Minor effect	Noticeable effect	Significant effect
29		eurdcyr	Not Applicable	No effect	Not Applicable	No effect	No effect *	No effect	No effect *	No effect *
30		eurdcdr	Not Applicable	No effect	Not Applicable	No effect	No effect *	No effect	No effect *	No effect *
31		eurdcmr	Not Applicable	Minor effect	Not Applicable	Minor effect	Minor effect *	No effect	No effect *	No effect *
32	# 9 dyn_pitch	eurcddyn	No effect	No effect	No effect *	No effect	Minor effect	Not Applicable	No effect	No effect
33		eurcldyn	No effect	No effect	No effect *	No effect	Minor effect	Not Applicable	No effect	No effect
34		eurcmdyn	No effect	No effect	No effect *	Minor effect	Noticeable effect	Not Applicable	Minor effect	Minor effect
35	# 10 dyn_roll_	eurcnpbh	No effect	No effect	No effect	Minor effect	Minor effect	Not Applicable	Minor effect	Noticeable effect
36		eurcrpbh	No effect	No effect	No effect	Significant effect	Significant effect	Not Applicable	Significant effect	Significant effect
37		eurcypbh	No effect	No effect	No effect	Insignificant effect	Insignificant effect	Not Applicable	No effect	No effect
38	# 11 dyn_yaw_	eurcnrbh	Noticeable effect	No effect	No effect	Minor effect	Noticeable effect	Not Applicable	No effect	Minor effect
39		eurcrrbh	Noticeable effect	Noticeable effect	No effect	Noticeable effect	Noticeable effect	Not Applicable	Noticeable effect	Significant effect
40		eurcyrbh	No effect	No effect	No effect	Insignificant effect	Insignificant effect	Not Applicable	No effect	No effect

* The table zeroing-out effect was inferred by association to the same effect in a different stall maneuver that was investigated, or from a table-group effect where the effect of one table was presumed to be dominant.
‡ For full wheel- and rudder-pulse inputs, the initial controls-neutral departure turns into a commanded roll-off or nose-slice departure, respectively. The table zeroing-out effect refers to the 'changed' departures.

Figure 20. Correlation matrix model parameter by their impact on the identified stall-departure aspects of the EURS

A descriptor for the power of each table to affect each of eight combinations of individual stall-departure aspects is noted above at the intersection of the corresponding row/column location. Any departure aspect affected by an individual table, whether alone or in a group, consists of the average of the observations, which may include synergisms between the combined tables. 'Not Applicable' entries apply to tables that are not directly related to the effect on particular stall-departure aspect or to the stall maneuver in which it occurs. For example, aileron and spoiler control-effectiveness tables do not affect stall-departure aspects in the stall maneuvers in which these control surfaces do not deflect (no wheel inputs).

One of the most significant findings was of a few EURS parameters that alone stood out as key elements in reproducing most of the individual departure aspects. Longitudinal static stability and control effectiveness had the most significant indirect impact on all the fully developed, post-stall departure aspects of the EURS. For example, just zeroing out the pitch-stability component alone in the stabilizer effectiveness table affected the fully developed post-stall, wing-rock departure aspect in all aft-CG stall maneuvers. It was an indirect effect because prevented the simulation from reaching the post-stall angle of attack where this departure aspect manifested itself. The elevator effectiveness pitching moment table had the same indirect effect.

3.2 RANKING OF MODEL PARAMETERS BY IMPACT ON STALL-DEPARTURE ASPECTS

The overall approach to the ranking of the EURS model parameters included the following:

- Review visual correlation results to discriminate between significant, noticeable, and minor impact on affected aspects of the baseline EURS stall-departure characteristics.
- Develop a numerical ranking method to resolve any ranking ambiguities and confirm visual ranking results. This numerical method would provide a more definitive way of judging the required parameter accuracy/range in the next subtask.
- Select stall maneuvers for which control inputs are nearly identical to control inputs in the baseline maneuver when possible to minimize phase shifts due to pitch-math-pilot control timing of the pull to full-aft column, and the control coupling effects from the roll-math-pilot wheel and yaw damper rudder activity.

Visual inspection of the time history and cross plot data, as cataloged in the correlation matrix (figure 19), formed the basis for the ranking of each of the 40 EURS parameters/tables by their impact on the EURS stall/post-stall departure aspects. The number of affected aspects and the degree to which they were affected contributed to the ranking assigned: high, medium, or low.

Figure 21 shows the power of the basic static pitching moment and drag parameters (tables eurdcmh and eurdcdh, respectively) to affect the stall/post-stall departure aspects in the commanded wings-level deep-stall maneuver #1. The red traces show the reference EURS baseline simulation. These examples highlight the differences in the individual effect, when zeroed out, of a high- and a low-rank parameter on the departure aspects of the same stall maneuver. The static lift parameter (eurdclh) had no effect at all on any of the departure aspects of this stall maneuver.

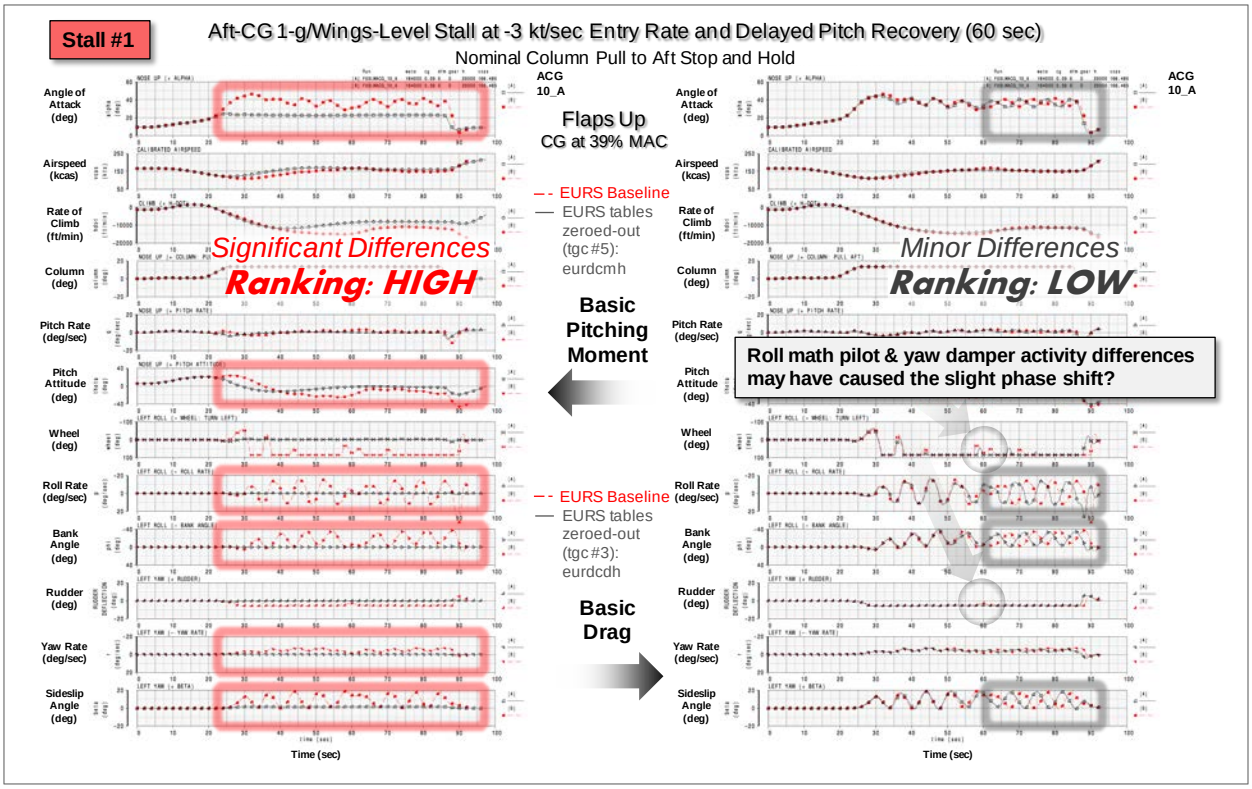

Figure 21. Examples of a high and a low visual ranking

The effect of the pitching moment parameter is dramatic. Neither the nose-slice departure in the initial stall phase nor the wing-rock in a slow, oscillatory-spiral departure in the fully developed post-stall phase occurs when the static pitching moment element in this EURS table is zeroed out. Conversely, the drag parameter has no effect in the initial phase of the stall and a minor effect in the later stages of the fully developed phase with a slight phase shift in the wing-rock departure with frequency and amplitude remaining unchanged. It was difficult to ascertain whether the observed phase shift was caused by roll-math-pilot and yaw-damper activity. In some cases, companion stall maneuvers with the roll math pilot and yaw damper on and off (stall maneuvers #7 and #8) were added to resolve these ambiguities.

Figure 22 illustrates the numerical scoring of five categories of basic flight parameters and their defining patterns, in time-history and cross-plot format, for two stall departure aspects in the initial stall phase and three in the fully developed post-stall phase. Loss or decay of lateral and directional control effectiveness and the post-stall-gyrations aspect were ranked by a similar scoring process using the time-history formats alone. Post-stall gyrations were scored by their absence in the time histories rather by their random presence.

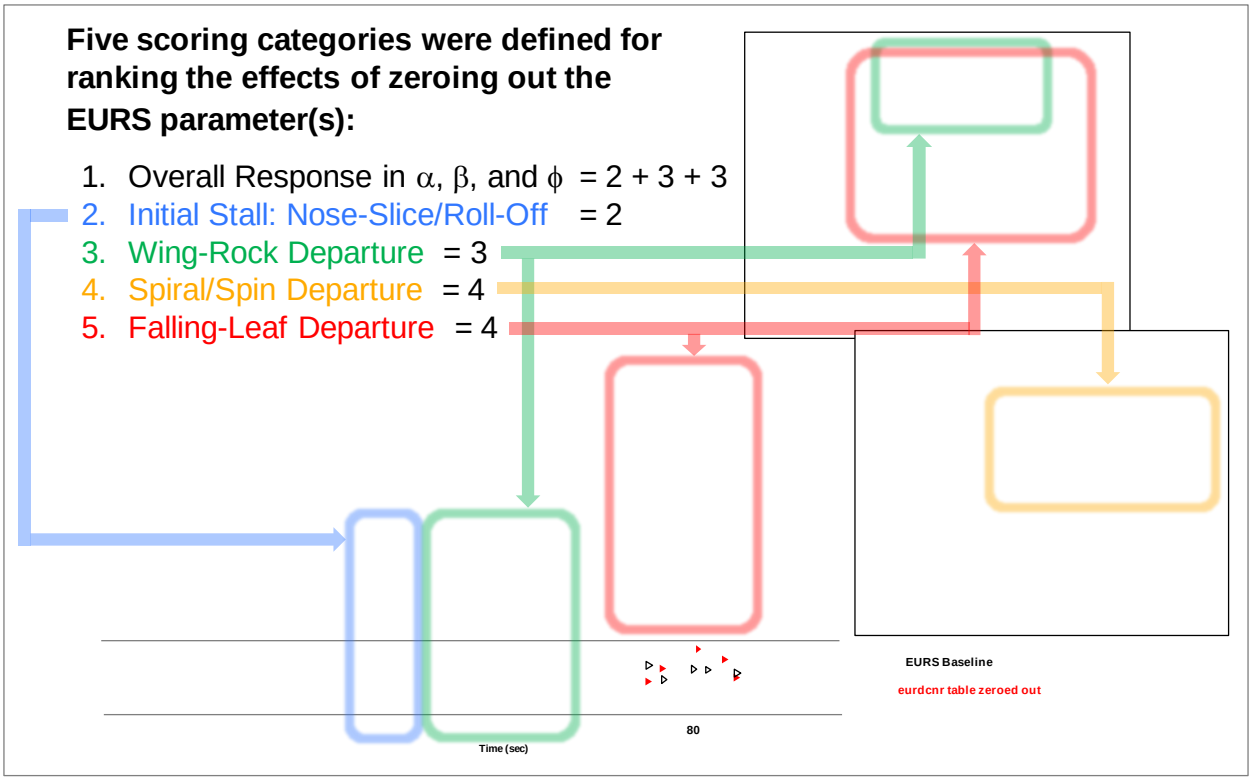

Figure 22. Examples of a high numerical ranking

The numerical ranking method was similar to the visual-inspection method in that it used the same QSD defining parameter-value relationships for the various aspects of a stall departure distributed across the different stall phases (figure 6) and the same plotted data. However, instead of a high, medium, or low rank, a numerical score from 1 to 4 was used to rate the power to affect the patterns and relationships of basic flight parameters defining each departure aspect. The number of aspects affected and the impact on the defining patterns and relationships as quantified by the 1 to 4 rating formed the basis of a total score compiled for each EURS parameter. A score of 4 denotes significant deviations in the pattern of the zeroed-out table/table-group traces (black) from the baseline EURS traces (red) in the respective phases of the stall departure being analyzed. A score of 0 or 1 denotes no deviations or minor deviations, respectively.

The primary discriminators in this process were steady-state value, phase shift, amplitude, frequency, and mean value in oscillatory behavior across time histories. The shape and orientation of the traces in the cross plots were primarily used in ranking the fully developed departure aspects. In this example, zeroing out the EURS rudder-effectiveness yaw parameter (table eurdcnr) results in an overall score of 23, a high-rank score above the medium/high gradation of about 20 based on correlations with the visual ranking results.

In the numerical ranking method, each departure aspect was systematically tracked and its deviation from these definitions scored. The scoring method used a set of rules applicable to that aspect based on its definition by patterns and relationships between the basic flight parameters when plotted in time-history format or cross plotted. The inspection was visual, but the scoring was numerical and could be summed so that the ranking would have a numerical basis with

traceability to the results of the EURS parameter correlation in Task 1.1. It was envisioned that the numerical scoring process would be more discriminating in the assessment of more subtle deviations in the QSD definitions when exploring the required accuracy of the EURS parameters in next task, Task 1.3. This process had the potential of resolving the finer gradations in the effect of measured changes to the EURS parameters, as compared to the more drastic change associated with the zeroing-out process used up to this point.

Both methods focused on stall maneuvers where random math-pilot/yaw-damper activity was minimal or absent (both turned off) to minimize cause-and-effect ambiguities. For example, turning stalls were sometimes useful because this maneuver, through and beyond stall, demanded full wheel and full yaw-damper rudder authority to maintain bank angle and turn rate, respectively.

A comparison between the numerical scores and visual ranking gradations established a relationship between the two methods. The numerical score could then be used reliably and systematically in the next subtask to determine parameter range and accuracy requirements. There were some differences in the rankings between the two methods, but overall they agreed well, as summarized in figure 23, which shows a comparison between the numerical score card results based on the scoring rules shown and the rankings from the visual inspection method.

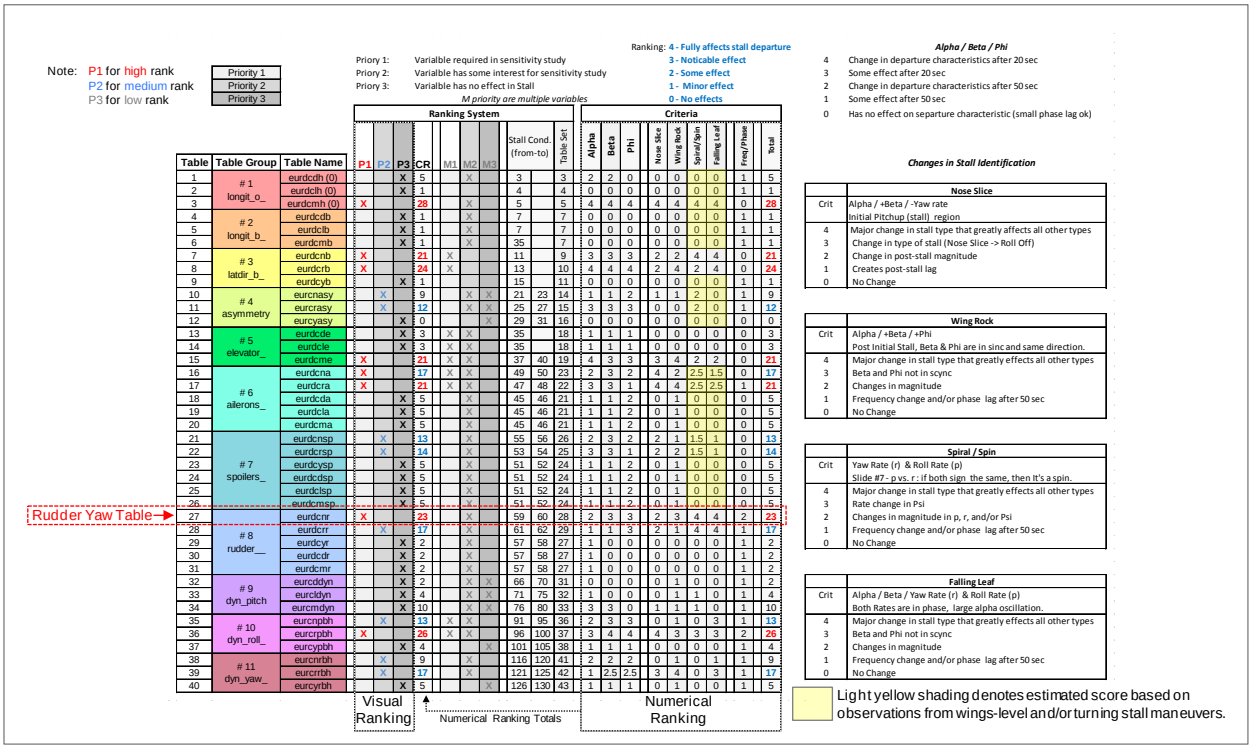

Figure 23. Summary of numerical ranking method and results

Table 1 compares the numbers of parameters visually ranked to those numerically ranked.

Table 1. Comparison of visual and numerical ranking methods

Ranking Level	Visual Method	Numerical Method
High (P1)	8 parameters	7 parameters
Medium (P2)	8 parameters	7 parameters
Low (P3)	24 parameters	26 parameters

While there are minor disagreements, the two approaches are reasonably consistent for distinguishing between the varying impacts of the individual parameters on the EURS stall departure characteristics.

3.3 ACCURACY STUDY OF TOP-RANKED PARAMETERS

The sensitivity in accuracy of the EURS model parameters for an acceptable level of stall and post-stall simulation fidelity was studied in the four-step sequence described in figure 24.

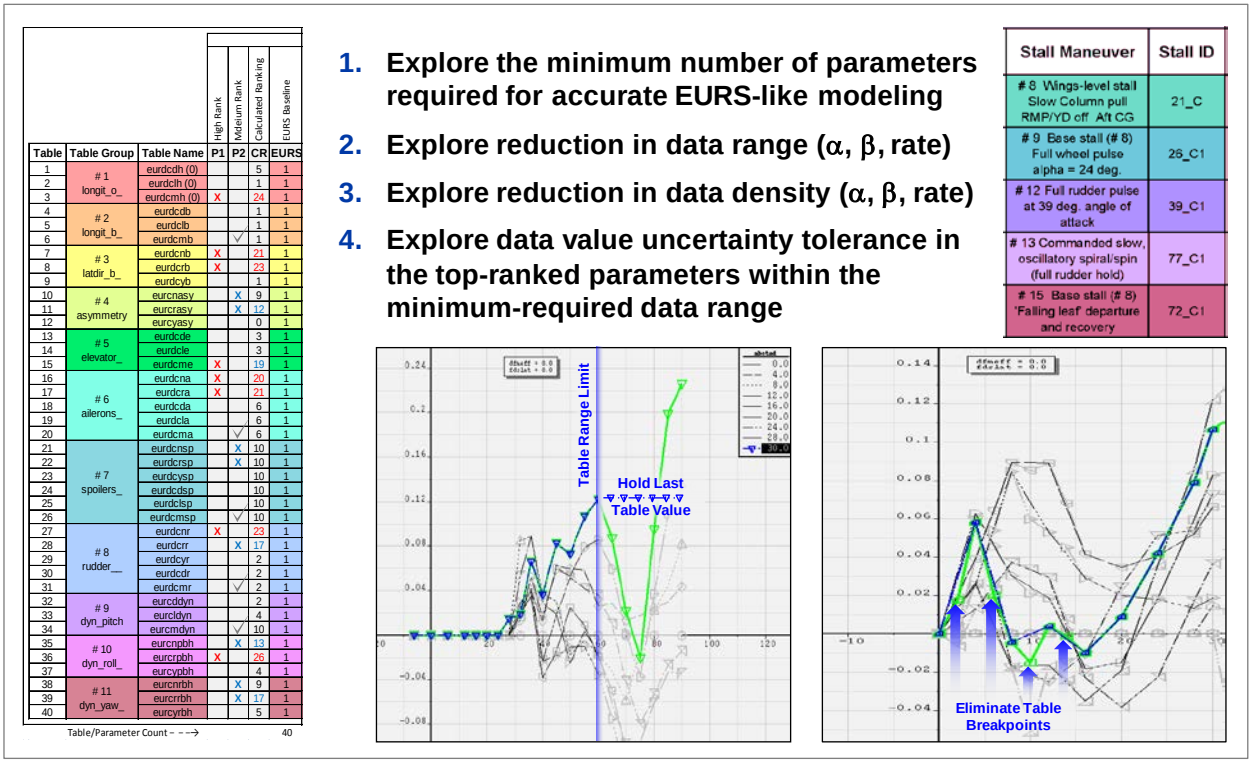

Table	Table Group	Table Name	P1	P2	CR	EURS
1	# 1 longit_o_	eurdcdh (0)			5	1
2		eurdclh (0)			1	1
3		eurdcmh (0)	X		24	1
4	# 2 longit_b_	eurdcdb			1	1
5		eurdclb			1	1
6		eurdcmb		✓	1	1
7	# 3 latdir_b_	eurdcnb	X		21	1
8		eurdcrb	X		23	1
9		eurdcyb			1	1
10	# 4 asymmetry	eurcnasy		X	9	1
11		eurcrasy		X	12	1
12		eurcyasy			0	1
13	# 5 elevator_	eurdcde			3	1
14		eurdcle			3	1
15		eurdcme	X		19	1
16	# 6 ailerons_	eurdcna	X		20	1
17		eurdcra	X		21	1
18		eurdcda			6	1
19		eurdcla			6	1
20		eurdcma		✓	6	1
21	# 7 spoilers_	eurdcnsp		X	10	1
22		eurdcrsp		X	10	1
23		eurdcysp			10	1
24		eurdcdsp			10	1
25		eurdclsp			10	1
26		eurdcmsp		✓	10	1
27	# 8 rudder__	eurdcnr	X		23	1
28		eurdcrr		X	17	1
29		eurdcyr			2	1
30		eurdcdr			2	1
31		eurdcmr		✓	2	1
32	# 9 dyn_pitch	eurcddyn			2	1
33		eurcldyn			4	1
34		eurcmdyn		✓	10	1
35	# 10 dyn_roll_	eurcnpbh		X	13	1
36		eurcrpbh	X		26	1
37		eurcypbh			4	1
38	# 11 dyn_yaw_	eurcnrbh		X	9	1
39		eurcrrbh		X	17	1
40		eurcyrbh			5	1

Figure 24. Analysis approach in exploring the sensitivity to modeling accuracy

The first step in this study explored whether the top-ranked parameters alone were sufficient to reproduce all aspects of the EURS stall and post-stall departure characteristics. These parameters are denoted in figure 24 by the red and blue X marks in the high-rank (P1) and medium-rank (P2) columns on the table insert to the left. The process used here was the inverse of that used in the correlation and ranking analysis. That is, all but the high-rank parameters/tables were zeroed-out, progressing to include the medium-rank (P2) tables, and then as many of the low-ranked tables

(with the rest zeroed out) as necessary until the EURS stall departure characteristics were reproduced with sufficient fidelity. The level of simulation fidelity was determined by the same rules and methods used in the visual and numerical parameter correlation and ranking described in the two previous sections.

Steps 2 and 3 are represented by the graphics at the bottom in which examples of data range and density reductions are visualized. The initial set of fifteen stall maneuvers was reduced to ten. As the study progressed, the stall maneuvers were reduced to five (upper right graphic). These five stall maneuvers were deemed sufficient to independently assess the effects of stability and control parameters.

This first step revealed that the minimum number of parameters required for accurate modeling of the aerodynamics in the EURS-like model rose from 16 high and medium rank parameters to 21. These 21 parameters in the EURS model were all moment parameters, which suggest that the force parameters have a secondary effect on the simulation fidelity of the EURS. The five low-rank moment parameters added are denoted in figure 24 by the grey check marks in the medium-rank column on the table insert to the left. There were four static parameters and one dynamic parameter added: sideslip-effects on basic pitching moment; the pitch-coupling parameters for ailerons; spoilers and rudder; and the pitch-damping parameter. These five additional parameters improved the simulation matches with either full-wheel or full-rudder inputs. The simulation of both the initial stall departure and fully developed stall departure aspects were improved.

The second step in the sensitivity-in-accuracy study determined how far the data range of the tables for these 21 parameters could be reduced while maintaining a comparable level of simulation fidelity as that achieved with all of these tables at full range.

In figure 25, the data grid of angle-of-attack and sideslip data is visualized for the EURS and non-EURS static models, and for the static wind-tunnel test data used in the development of the EURS model. The EURS model was developed by blending the wind-tunnel data values for a given parameter into those of the corresponding non-EURS model parameter starting at approximately 20º of angle of attack and of sideslip. A table of increments was then generated by subtracting the non-EURS parameter values from those of the blended EURS parameter. In the EURS model buildup equations, as illustrated in figure 17, this table of increments is added to the non-EURS model parameter term to generate the EURS model parameter values. Range reductions applied to this incremental ΔEURS table would be reflected accordingly in the EURS model parameter.

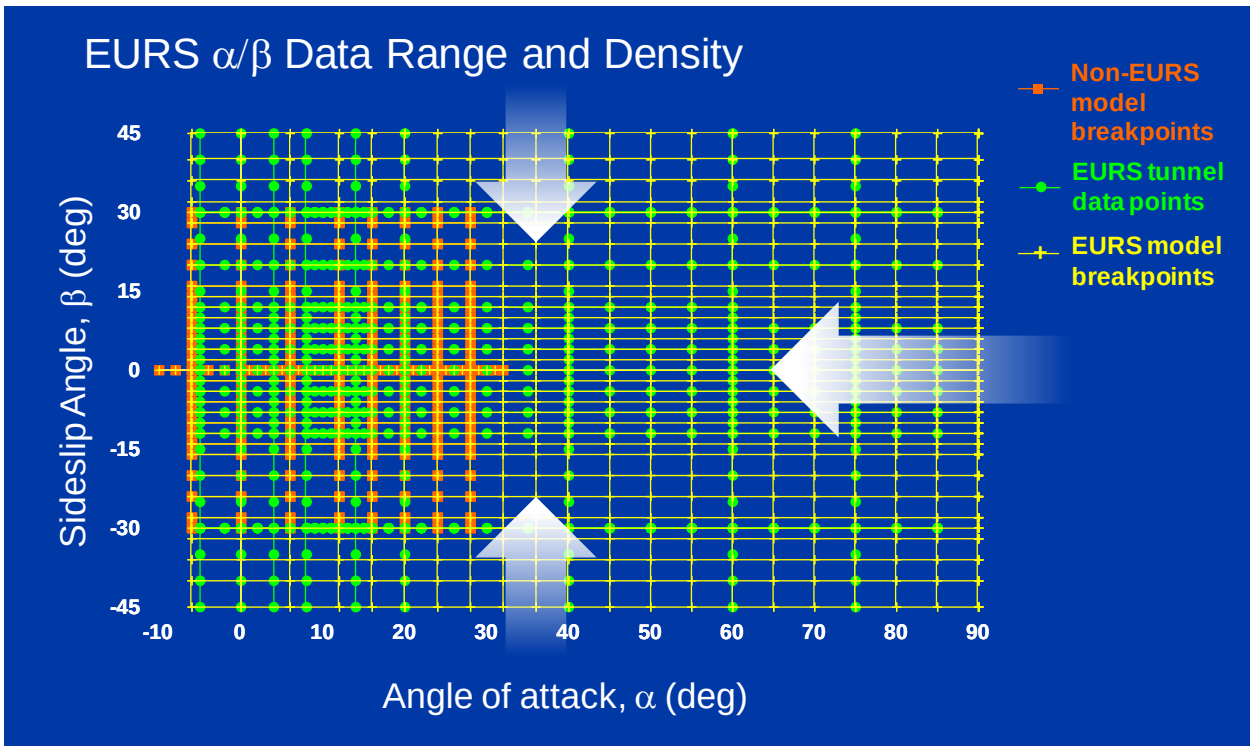

Figure 25. Analysis approach in exploring reductions in static data range

The approach was to first progressively reduce the positive angle-of-attack range of the medium-rank static tables to determine the minimum range required to provide adequate simulation fidelity. Verification of this minimum range on both the medium- and high-rank tables followed with adjustments to it if required. Once the minimum-required positive range in angle of attack was determined, the same process was followed for the sideslip range keeping the original, full angle-of-attack range. As a final check, both the minimum angle-of-attack and sideslip ranges were applied and adjusted as required. All dynamic tables were at full range throughout this process.

The same general approach was adopted to determine the minimum-required rate range in the dynamic moment tables, adopting the minimum-required range of 60º in angle of attack determined for the static tables. The static tables were kept at this range for consistency in the rate-reduction progression. Range reduction in angle of attack below 60º of angle was not explored because there are pronounced nonlinearities with rate introducing unstable-to-stable dynamic stability reversals at low rates between 35º and 55º angle of attack. The roll-damping parameter (the only dynamic parameter ranked high) appears to be linked directly to the wing-rock motion present in most EURS post-stall departures. Figure 26 illustrates the progression to the lower rate limits studied. For the dynamic tables, the reductions were aligned with the actual wind-tunnel-tested rates to have a more direct correlation to the reduction in data requirements relative to the EURS forced-oscillations testing.

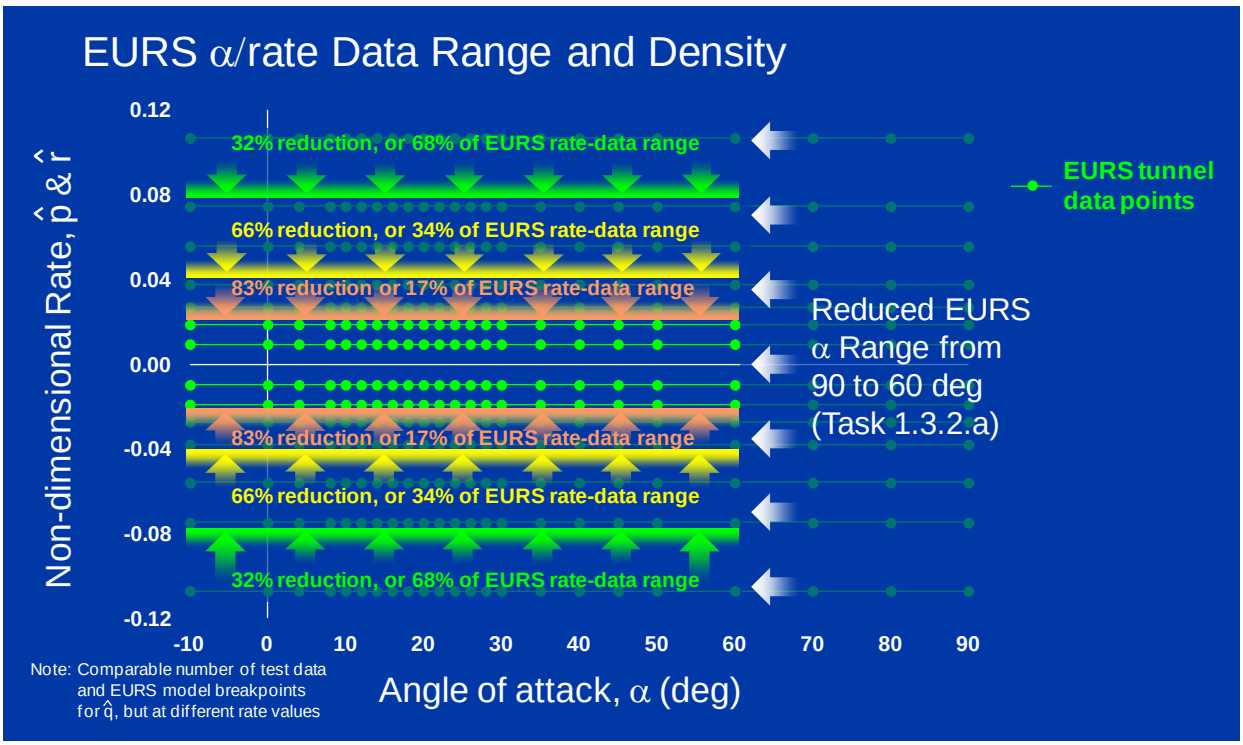

Note: Parameter values and rates in body axes.

Figure 26. Analysis approach in exploring reductions in dynamic data range

Figure 27 shows the rolling moment parameters due to roll rate and yaw rate at 30º and 40º angle of attack. In the plot, at 40º angle of attack, the unstable-to-stable reversal in the roll-damping (roll due to roll rate) between 35º and 55º angle of attack is evident at low rates. A similar trend is present in the roll-coupling with yaw rate parameter. The effect on the modeling accuracy of this particular trend in these two parameters is visualized here for each step in the rate-reduction process. The extrapolated values beyond the reduced ranges reflect the dynamic-derivative nature of the underlying non-EURS baseline model.

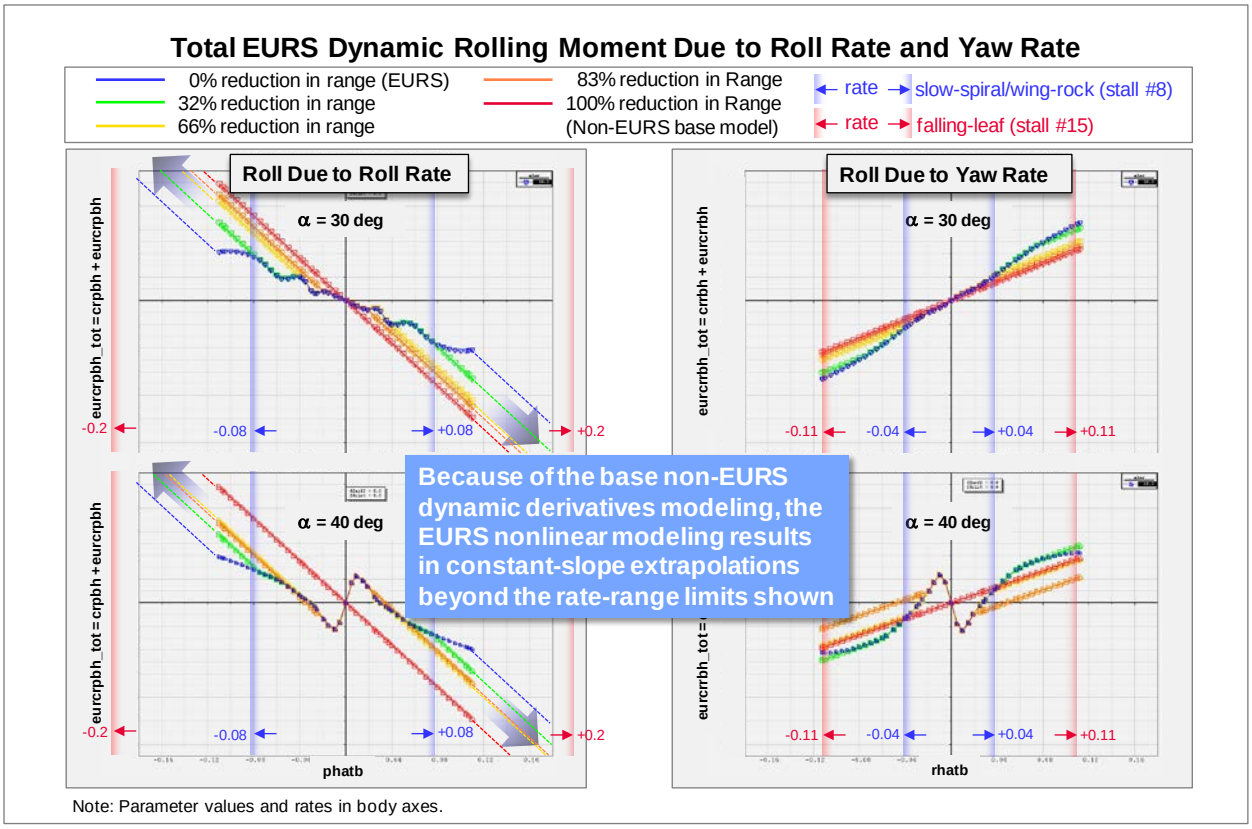

Note: Parameter values and rates in body axes.

Figure 27. Nonlinearities in roll-rate dynamic parameters at 30º and 40º angle of attack

Summarizing the results of the parameter-range study, the minimum range required to provide a comparable level of simulation fidelity as that achieved with the 21 EURS moment tables at full range was as follows:

- Angle of attack up to 60º (reduced from 90 in the EURS)
- Sideslip angle out to ±30º (reduced from ±45 in the EURS)
- Nondimensional roll and yaw rate out to ±0.075 (reduced from ±0.110 in the EURS)
- Nondimensional pitch rate out to ±0.005 (reduced from ±0.0075 in the EURS)

These minimum-required ranges provide the same level of fidelity as that achieved with all 21 required tables at full range. Further reductions in range degraded simulation fidelity to an unacceptable level of the post-stall departure aspects where angle-of-attack, sideslip, and rate excursions exceeded these data-range boundaries.

After the minimum-required ranges were established, the third step in exploring the sensitivity in accuracy of the required parameters explored how much the density/resolution of the data could be reduced while maintaining a comparable level of simulation fidelity as that achieved with these tables at full range and density.

The approach was to progressively reduce the data density in angle of attack of the static tables by first removing every other angle-of-attack table breakpoint, as illustrated in figure 28 for the minimum-required data ranges. The intent was to repeat this progressive reduction process until the minimum-required data density in angle of attack was determined based on the same simulation fidelity requirements previously used to determine minimum-required ranges. As in the range-reduction process, the minimum acceptable data density for the medium-rank static tables was determined first, followed by verification of this minimum range on both the medium- and high-rank tables with adjustments if required. Once the minimum-required data density in angle of attack was determined, the same process was repeated for the sideslip data.

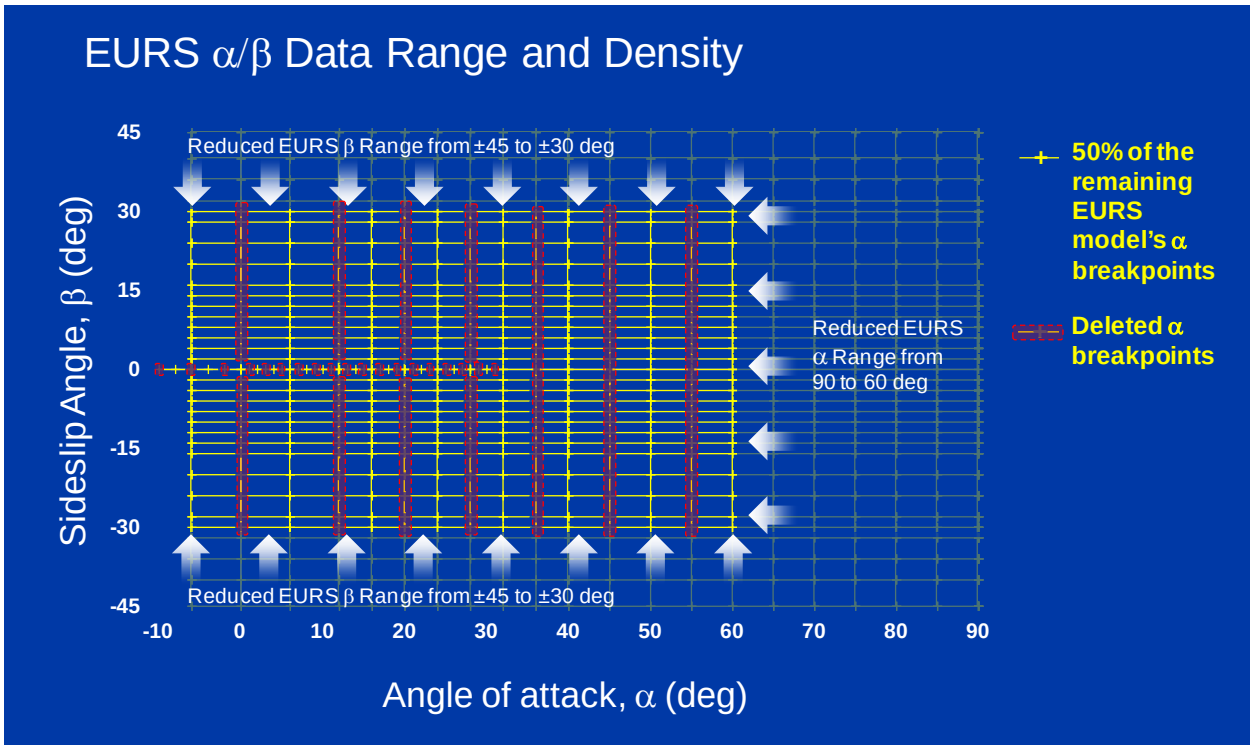

Figure 28. Analysis approach in exploring reductions in static data density

In the first reduction step of this process, starting with the medium-rank tables, it was found that angle of attack in the EURS model was already at minimum density. Removing every other angle of attack data point in the medium-rank tables alone resulted in unacceptable simulation fidelity of the stall departure aspects in both the initial and post-stall phases of the stall maneuvers investigated.

Proceeding to determine the minimum-required data density in sideslip revealed that sideslip density could be reduced by 50%, such that the typical sideslip spacing of 2º between table breakpoints could be increased to 4º. This is significant in that the denser angle-of-attack and sideslip wind-tunnel data grid gathered for the EURS model development (green data grid in figure 25) could be greatly reduced. The mix of sideslip sweeps at constant angle of attack and angle-of-attack sweeps at constant sideslip in the EURS testing could be simplified for the development of an EURS-like aerodynamics model by gathering all the required sideslip-effects data with angle-of-attack sweeps alone at every 4º of sideslip up to the required-minimum range.

The data density of the dynamic (forced-oscillation) testing for the EURS model is illustrated in figure 28 within the angle-of-attack and rate-data envelope that would be required in the development of an EURS-like model. In the typical non-EURS dynamic-derivative models of transport airplanes, most of the stall and post-stall nonlinearities that may exist with both angle of attack and rate are not captured by the analytic methodology used in developing such models. Therefore, it is recommended that dynamic test data be gathered at the EURS angle-of-attack and rate density until there is more insight gained into these nonlinearities from accurate analytic methods or additional test-based knowledge for this type of airplane. However, reductions in angle-of-attack density may be contemplated if the nonlinearities with angle of attack near stall have already been captured by a more accurate analytic dynamic-derivative model or by flight-update adjustment of a less accurate model. A similar reduction in rate density, particularly in the roll-rate parameters, may be possible if the nonlinear unstable-to-stable reversal feature in the EURS roll-damping modeling, highlighted in figure 28 is a common aerodynamic characteristic in this type of airplane.

Summarizing the results of the parameter density study:

- EURS data density in angle of attack should be maintained in both the static (figure 25) and the dynamics model parameters (figure 26).
- EURS sideslip data density can be reduced to every 4º of sideslip and still maintain adequate stall and post-stall simulation fidelity.
- EURS dynamics model nonlinear variations with angle of attack and rate are sufficiently different from those of the equivalent dynamic-derivative model (insert in figure 29) such that any reduction in angle of attack and rate density should be avoided.

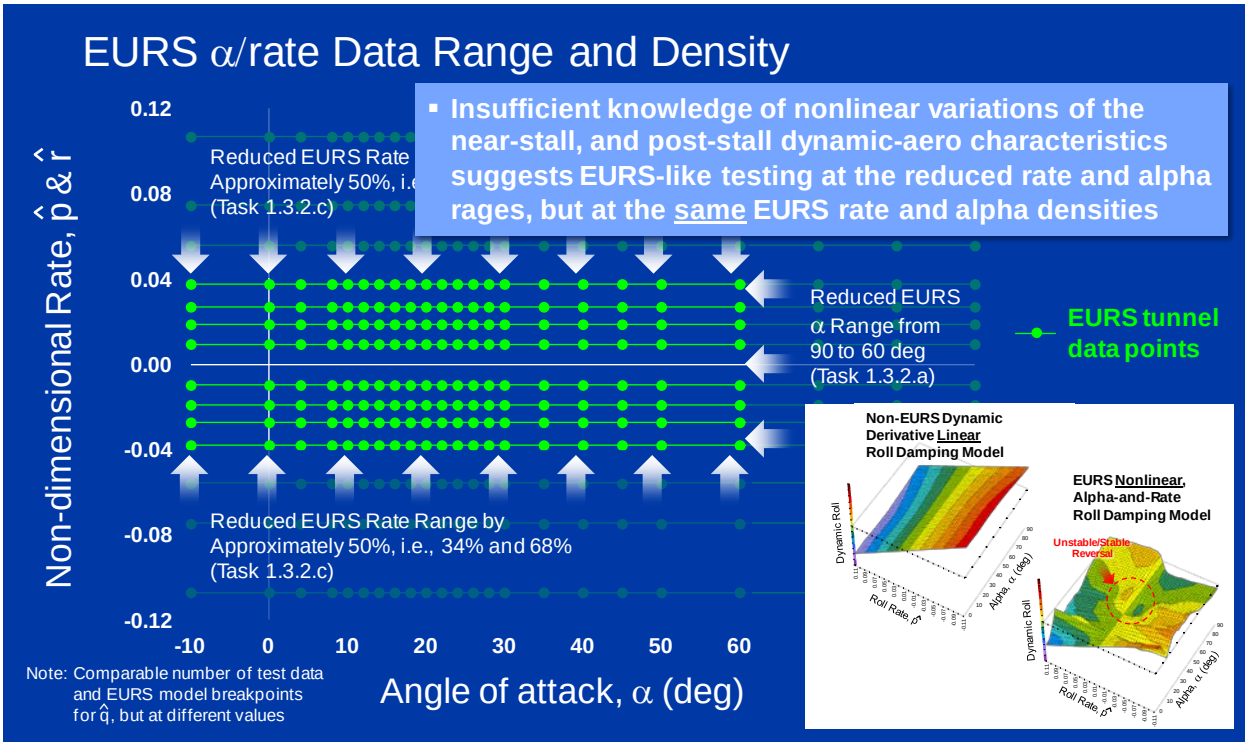

Note: Parameter values and rates in body axes.

Figure 29. Reductions in dynamic data density

After the minimum-required data range and density for an EURS-like aerodynamics model were established, the fourth and final step in the sensitivity-in-accuracy study was to determine the required accuracy in the data values of the 21 required moment parameters within the minimum-required range boundaries. Figure 30 depicts the angel-of-attack and sideslip static data ranges under consideration. A baseline non-EURS model typically has reasonable accuracy and stall simulation fidelity up to 30º angle of attack and ± 30º of sideslip. A candidate EURS-like model would require an expanded range of accurate data up to 60º angle of attack.

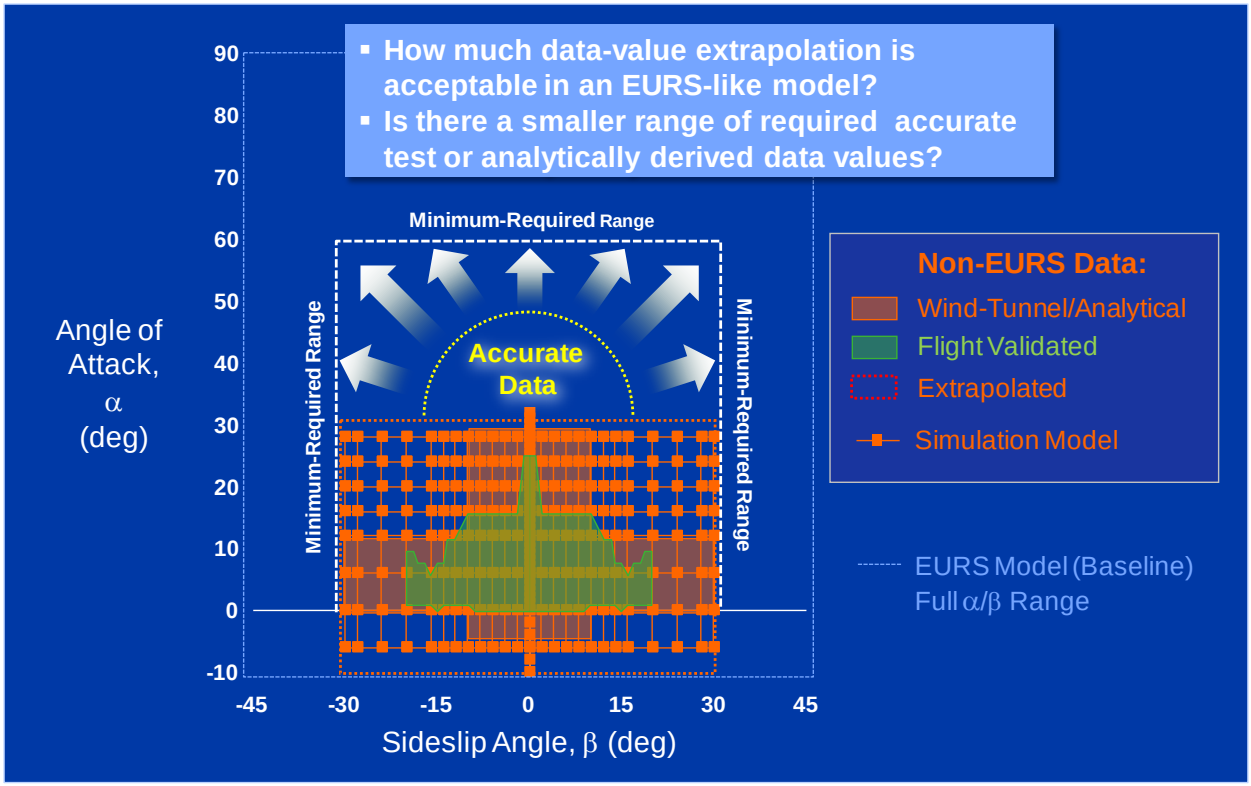

Figure 30. Candidate data regions for extrapolation

The following questions shaped the analysis approach developed to determine the accuracy requirements of these data:

- Can the data trends from within the non-EURS model range be extrapolated up to the minimum-required range of a candidate EURS-like model and still provide sufficient simulation fidelity?
- If so, is there a reasonable envelope of uncertainty or percent-error from the actual EURS data values in this unknown-data region that will allow this?
- If not, is there a smaller region of accurate data between the non-EURS baseline range and that of the minimum-required range of a candidate EURS-like model that will?

The process of establishing the minimum parameter ranges requiring accurate data revealed that the lower ranked moment parameters required accurate data across a narrower range of angles of attack and sideslip. The high-rank parameters alone dictated the wider range of accurate data: the minimum-required range. Reducing their range to match that of the lower ranked parameters resulted in loss of simulation fidelity. Based on these findings, two reduced regions of accurate data were considered. Figure 31 illustrates these two regions. Region 1 represents the region of accurate data that was required for medium-rank parameters as long as the high-rank parameters were accurate up to the required-minimum range. Extrapolation of the high-rank parameter from the accurate values within the bounds of Region 1 was explored to determine the level of inaccuracy that could be tolerated while providing adequate simulation fidelity. A growing level of inaccuracy from Region 1 to ±10% inaccuracy in the EURS model parameter values at the

minimum-required range was investigated. Acceptable simulation results with parameter values defined by the ±10% inaccuracy envelope would certify these as the boundaries within which extrapolated trends would be acceptable.

The same approach was repeated from Region 2, which represents the range of accurate data of a typical baseline non-EURS model.

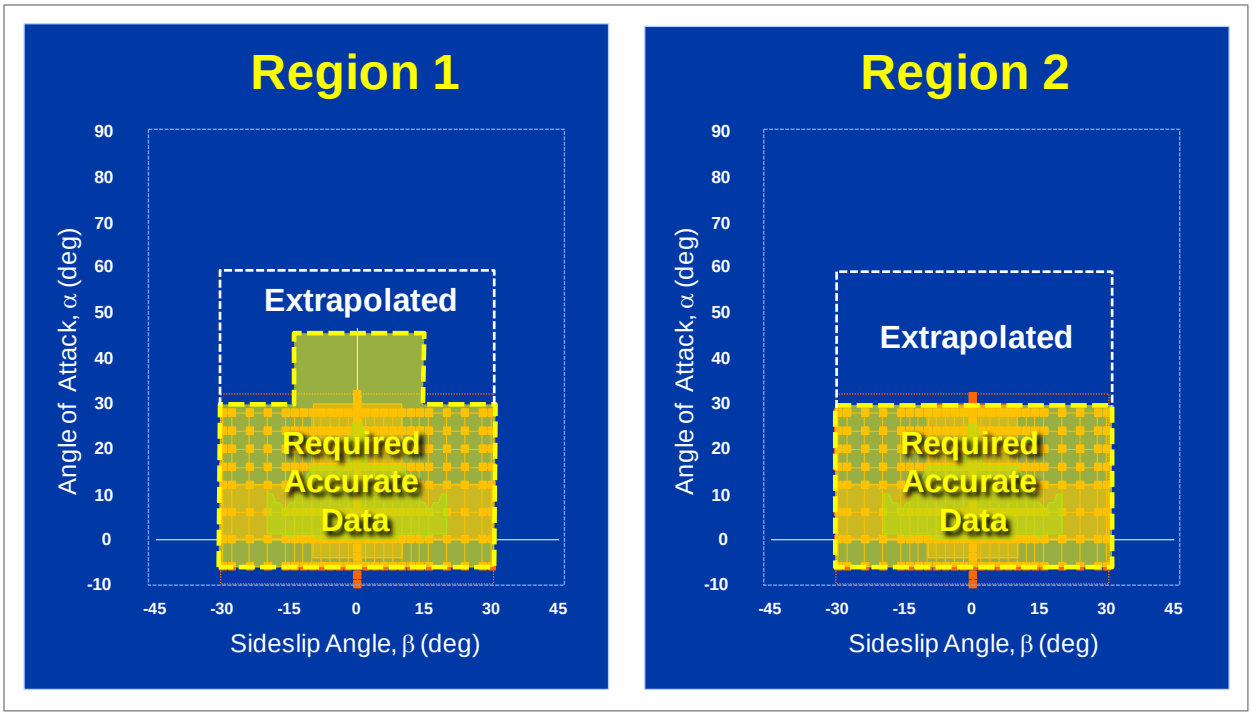

Figure 31. Regions of required accurate data considered in exploring tolerance to inaccuracy in extrapolated regions

The example in figure 32 shows the ±10% inaccuracy envelope (green and yellow curves) around the EURS model values for the pitching-moment parameter (blue curve), one of the three high-rank, static stability parameters. This envelope was developed around the total values of this EURS parameter (eurdcmh_tot) as depicted in each plot at the top. A pair of incremental ΔEURS tables (eurdcmh) corresponding to the positive and negative envelope curves (plots at the bottom) were then generated by reversing the EURS parameter build-up process (figure 17). Plots on the left show the inaccuracy envelopes calculated for Region 1, applying a multiplicative ±10% inaccuracy function represented by the insert; those on the right are for Region 2.

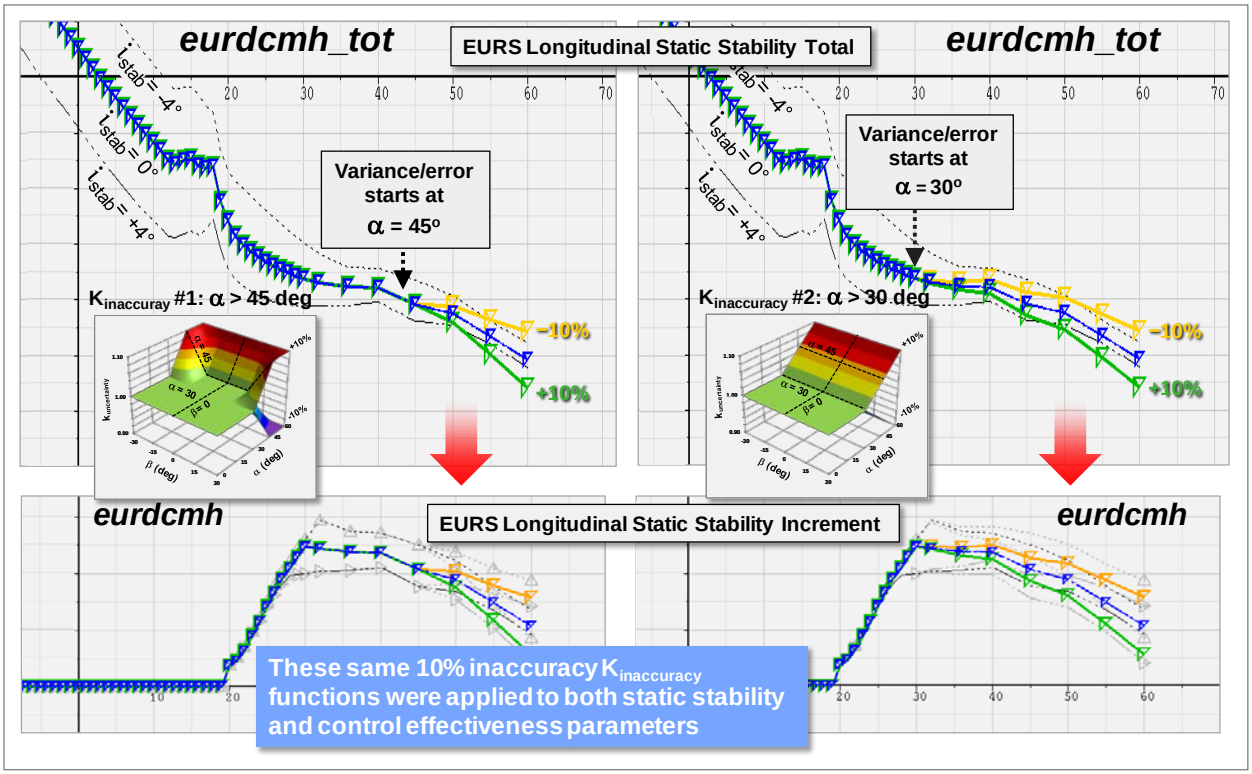

Figure 32. Example of ±10% inaccuracy envelopes for the longitudinal static stability parameter

The same process of applying ±10% variance/error ramps to the total values and then generating the corresponding incremental ΔEURS tables was used for the rest of the high-rank static stability and control effectiveness parameters, and the one high-rank dynamic stability parameter: roll damping. Figure 33 shows the ±10% inaccuracy envelopes and corresponding inaccuracy functions, applied as a multiplicative factor to the total values of the roll-damping parameter. From left to right, the inaccuracy functions represent progressively larger regions of unknown data with the last one being representative of exploring the acceptability of the a 10% level of uncertainty in developing an EURS-like model by simply adding the incremental ΔEURS table directly to the corresponding non-EURS baseline model.

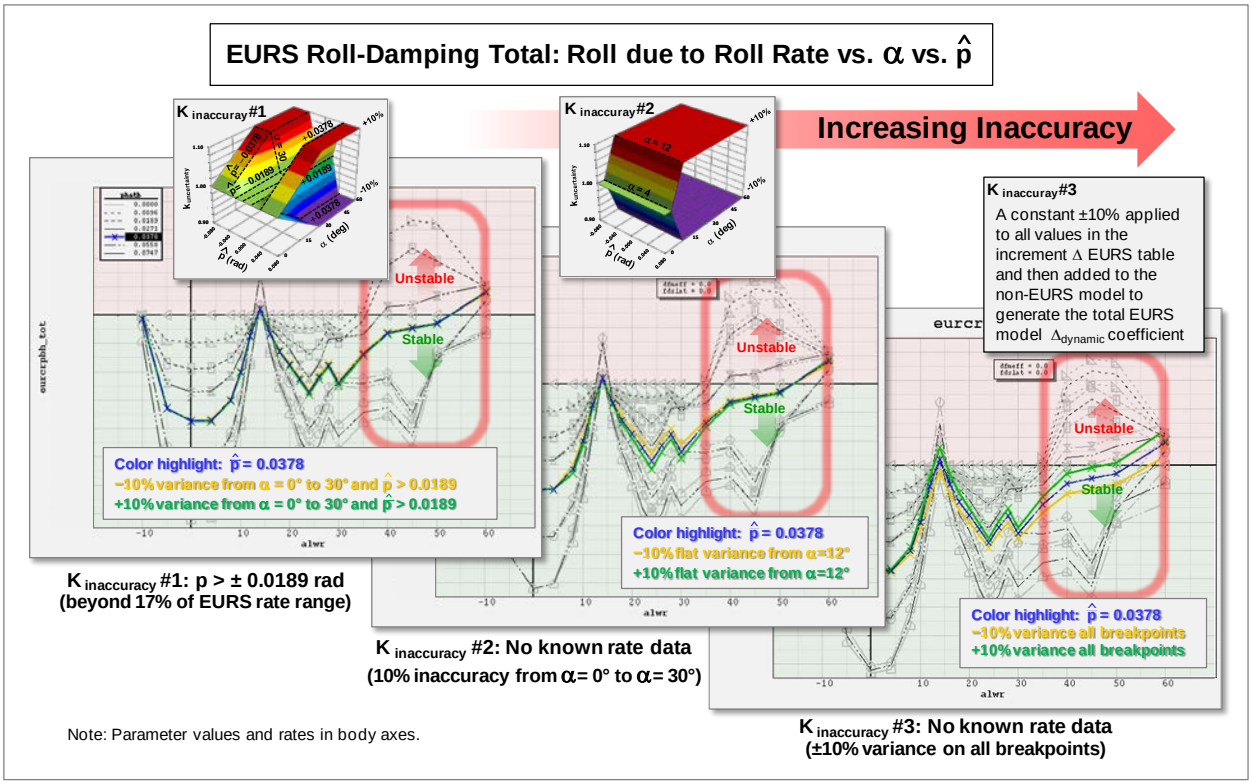

Figure 33. Example of ±10% variance/error envelopes for the roll-damping dynamic stability parameter

The effect on simulation fidelity with data values along the ±10% inaccuracy envelopes was determined individually for each of these parameter groupings. Results showed that this level of inaccuracy in the static parameters was acceptable in providing sufficient simulation fidelity when extrapolating from accurate data in Region 1, but not Region 2.

This section specifically addressed the range and density (or resolution) of the data, and the accuracy in data values required to develop an EURS-like aerodynamics model of a transport airplane similar to that modeled by the EURS. In a simulation environment, such a model would reproduce the stall and post-stall departure characteristics of the airplane modeled. The fidelity of these simulations will be driven by reductions in the range and density of accurate aerodynamic data and the ability to extrapolate beyond the range of the accurate data up to the minimum-required range of such a model.

These requirements are sufficient to develop an EURS-like aerodynamics model of a large jet transport similar to that modeled by the EURS. When doing so, the following additional considerations should be kept in mind:

- Model accuracy, particularly in pitch stability and control effectiveness, is paramount in reproducing the correct full-stall or post-stall angle of attack across the simulated CG range.

- EURS nonlinear dynamic characteristics with angle of attack and rate may not be common to all conventional twin-jet transports (e.g., the unstable-to-stable reversal in roll damping in a deep stall).
- Steady wind-axes rotational effects (rotary-balance test data) were not modeled and, therefore, their effect on fully developed spin modes could not be determined.

The requirements set forth here were the basis for the work in Task 2 of this phase, in which the cost of wind-tunnel testing and post-test data-processing analysis, was weighed against the savings of reduced testing and the additional costs of analytical extrapolation and blending required to supplement testing at a reduced data range and density.

3.4 ASSESSMENT OF ANALYSIS VS. WIND TUNNEL TESTING

To assess the potential to limit wind-tunnel test costs while providing the required data-density and accuracy levels discussed above, analysis methods were explored to determine which EURS parameters can be developed with a minimized test program. With current CFD capabilities being insufficient and impractical for the fully separated flow regimes modeled by the EURS, various extrapolation techniques were considered as the potentially viable analysis techniques. Simple linear extrapolation of an accurate baseline dataset, extrapolation of an accurate baseline dataset guided by large-incidence-angle aerodynamic approximation methods (where applicable), and extrapolation using the current EURS database as a guide were all considered.

The previous work concluded that accurate data (i.e., test-based data) is not needed in the entire range of required data and that up to ±10% of inaccuracies at the angle-of-attack and sideslip minimum-required range boundaries would be acceptable. In most cases, accurate data were only required out to the bounds of Region 1 (figure 31). Accordingly, this region was the baseline used for the evaluation of potential analytic extrapolation methods; however, a few parameters were identified in which extrapolations from Region 2 were considered based on results of this evaluation.

Extrapolation options for the basic pitch, roll, and yaw static-stability parameters are explored in figure 34. Potential extrapolations are shown in the red-dashed lines and accuracy bounds are provided by the three colored lines, assuming accurate data in Region 1 (figure 32). Simple visual inspection shows that pitch-stability characteristics can be extrapolated with simple linear extrapolations, but that more advanced techniques are required to meet the accuracy requirements in roll and yaw stability. The large-incidence-angle aerodynamic approximations considered sets the target values for the extrapolation, and blending is performed from the bounds of accurate data (Region 1). The theories applied are based on the variation of the resultant normal force with airflow incidence at large angles of attack and sideslip, as applicable to the individual airplane components, and taking into account their respective moment arms. The flow incidence angles for the zero and maximum values of the resultant normal force became the anchor points for the normal force and the corresponding moment calculations. Simple sine and cosine relationships with estimated local flow-incidence angle were used to calculate the trend in the generated moments by each airplane component. Extrapolating using this approach did not prove fruitful for the roll and yaw stability parameters because it does not capture the non-linearities in both angle of attack and sideslip within the required accuracy bounds. The only practical option for extrapolating requires the EURS data trends to shape these parameters in a new EURS-like model

using the accurate data as the anchor point to blend in the EURS trends. For the roll- and yaw-stability parameters, it is expected that these are reasonable approximations for similarly configured transport-category airplanes.

Collecting static-stability data in Region 1 does not provide the data required to generate the stall asymmetries modeling in the EURS. A review of the roll and yaw asymmetries modeled by the EURS show that there are significant variations with angle of attack in these two important components up to and above 45º angle of attack. These variations are highly nonlinear and may not be captured by any analytical extrapolation or blending of EURS trends. Therefore, data collected for the basic lateral/directional stability parameters should have an extended range in angle of attack up to 60º across and ±8º of sideslip at which these stall asymmetries manifest themselves.

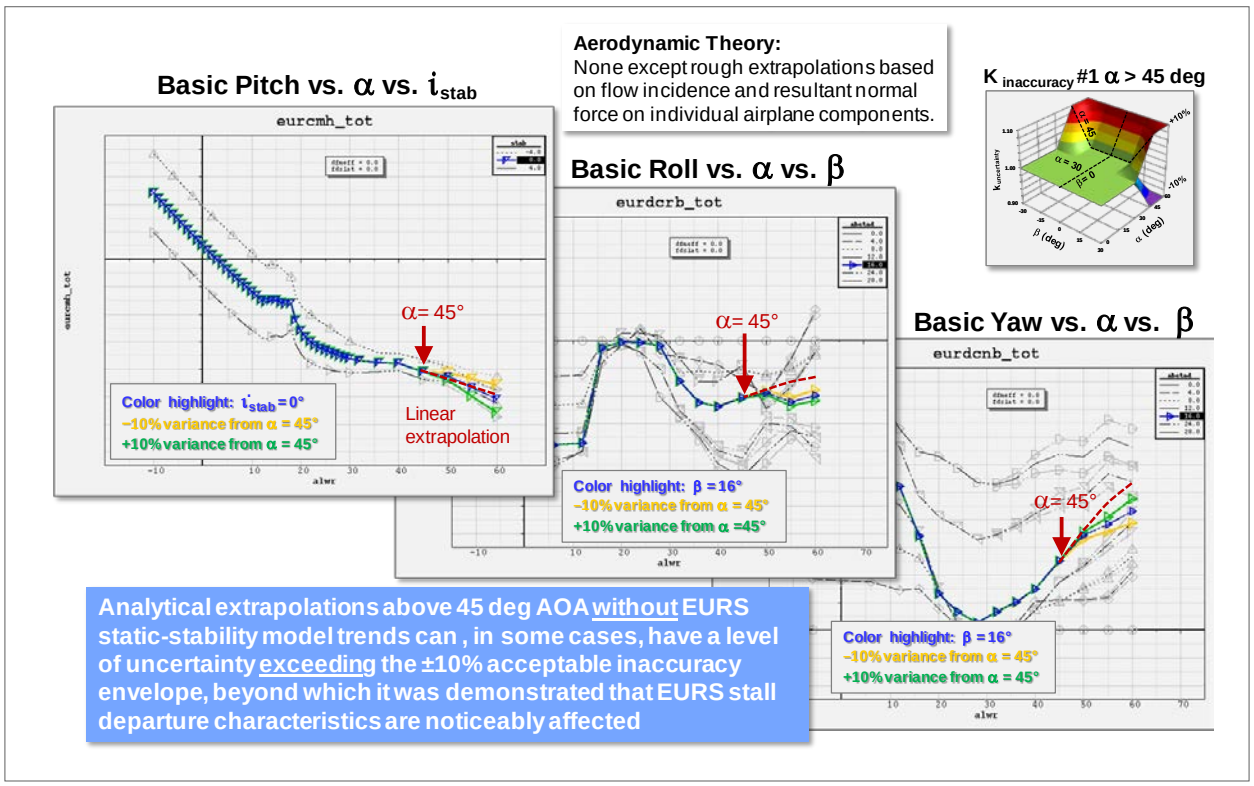

Figure 34. Extrapolation assessment of static-stability parameters

Potential control-surface extrapolations were explored for elevator and rudder, as illustrated in figure 35. The large-incidence aerodynamic theory applied to control surface effectiveness identifies the zero or minimum-control surface effectiveness by estimating the angle of attack or sideslip at which airflow incidence is normal to the corresponding wing or tail surface, or it is aligned with the control-surface hinge line. In shaping the extrapolated variation with angle of attack and sideslip of the tail control surfaces, approximate wake effects from wing and fuselage are included. Stall-incidence angles of wing-tail surfaces are taken into consideration where applicable, but these are mostly within the accurate data region. For the elevator and rudder, the high-incidence aerodynamic theory and simple linear extrapolations produce similar results over the extrapolation window considered. Given the characteristics of the rudder-effectiveness terms,

these parameters are candidates for extrapolation from Region 2, using the high-incidence aerodynamic theory and engineering judgment. Conversely, even from Region 1, the elevator extrapolation fails to remain within the required accuracy bounds. The trend developed based on the high-incidence theory estimates of zero/minimum control effectiveness at 90º angle of attack was not sufficiently accurate. This and the importance of elevator effectiveness in determining maximum post-stall angle of attack requires the EURS data trends to shape these parameters in a new EURS-like model. The stabilizer effectiveness component of the static-stability parameter requires similar treatment because it can have the same effect on the maximum post-stall angle of attack across the CG range. Similar assessments were performed for the lateral control surfaces. For the ailerons, extrapolation using the appropriate modifications of the EURS trends is required to provide acceptable accuracy. Given the lesser contributions of the spoilers to roll control at high angles of attack, it was found that the spoilers can also be extrapolated from Region 2 using high-incidence aerodynamic theory and engineering judgment.

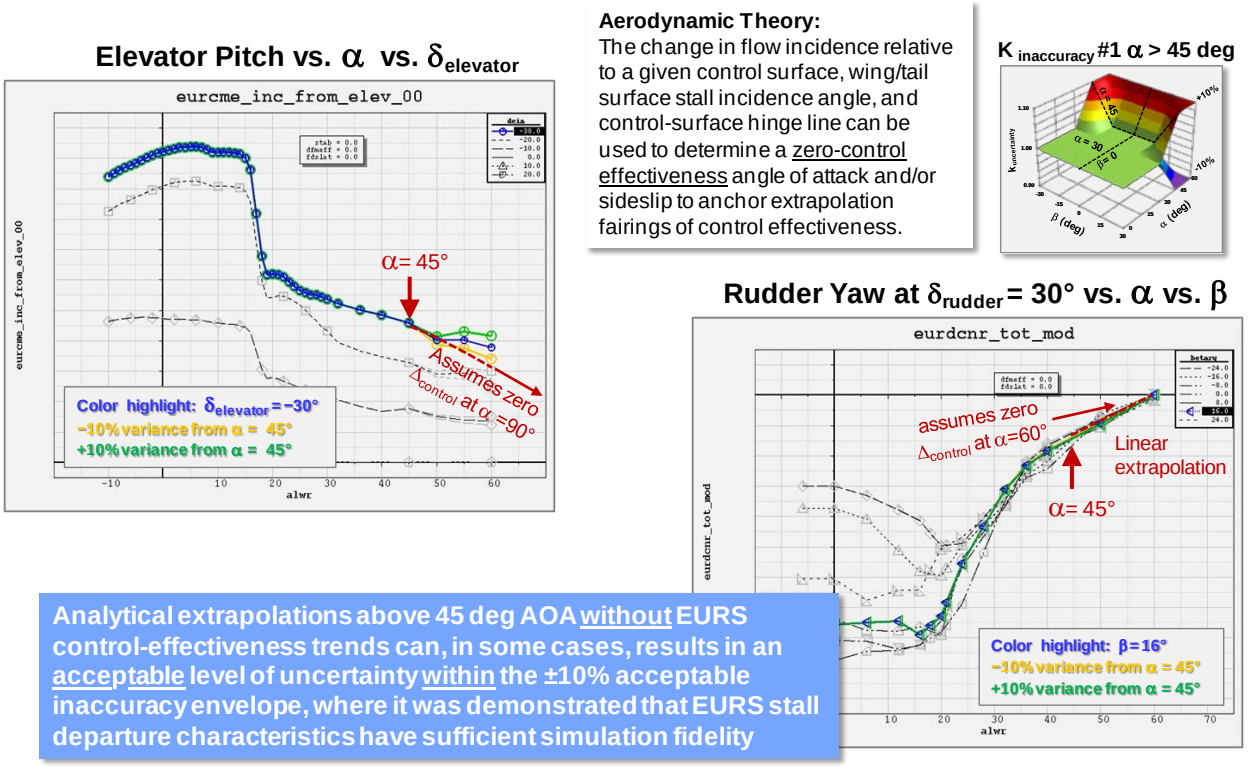

Figure 35. Extrapolation assessment of control-effectiveness parameters

The dynamics modeling previously showed that there are critical stable-to-unstable damping characteristics in some of the high- and medium-rank parameters at the higher angles of attack that were under consideration for extrapolation. Accepting degraded accuracy in those regions risks mischaracterizing the those critical components and degrading simulation fidelity. Visual inspection of figure 36, which shows extrapolation candidates for roll damping, shows that linear extrapolation does not meet the accuracy requirement—the highlighted condition shows a marginal ability to meet the least accurate requirement considered (plot on lower right), and more pronounced non-linearities across the rest of the rate-data space (not highlighted) that would not be captured with linear extrapolation. With no viable high-incidence aerodynamic theory to apply,

the only other analysis option would be to apply the trends from the EURS model to future models. At this time, it cannot be said with confidence that these characteristic shapes would carry across to other similarly configured transport airplanes unless the two configurations were extremely similar. Accordingly, it is recommended that extrapolation not be considered for a majority of the dynamic derivatives. One exception is pitch damping, a low-rank parameter that could be extrapolated from Region 2 because the trends in this modeling component do not show significant non-linearities, and extrapolation guided by the EURS trends can be applied. If dyanmic data of this type are collected for a wider range of transport-category airplane models, it is possible that analytic methods could be developed, which may be confidently used in extrapolation techniques using common trends identified in this larger volume of dynamic data..

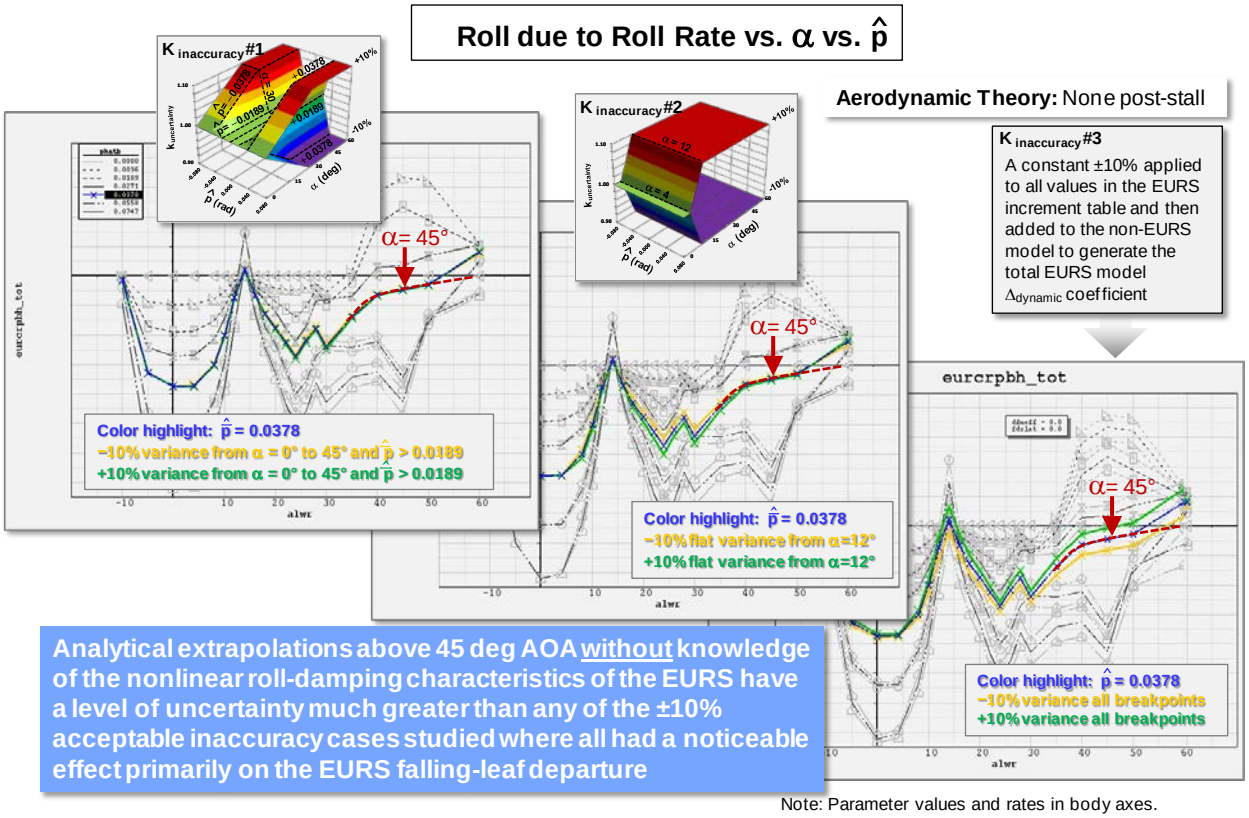

Note: Parameter values and rates in body axes.

Figure 36. Extrapolation assessment of the roll-damping dynamic stability parameter

The summary in table 2 shows which tables can accept a reduced region of accurate data while having a viable approach for using analysis to extend the data range to the minimum-required data boundaries. The regions defined in the table are in reference to those defined in section 3.3 and illustrated in figure 31; “N/A” indicates that no viable technique is available to extend the data from a reduced region to the bounds of the minimum-required data set. This summary is used to develop appropriately sized wind-tunnel test plans for new EURS-like models while providing adequate simulation fidelity.

Table 2. Summary of reduced regions for accurate data and analysis techniques

Table Name		Reduced Region of Accurate Data	Recommended Analysis Technique
Static Stability	eurdcmh (P1)	Region 1	EURS-guided extrapolation
	eurdcmb (P2)	Region 1	EURS-guided extrapolation
	eurdcnb (P1)	Region 1	EURS-guided extrapolation
	erudcrb (P1)	Region 1	EURS-guided extrapolation
	eurcnasy (P2)	N/A	Extrapolation not viable for small sideslip angles (□< +/- 8)
	eurcrasy (P2)	N/A	Extrapolation not viable for small sideslip angles (□< +/- 8)
Control Surface	eurdcme (P1)	Region 1	Linear extrapolation or Large-Incidence Aero Extrapolation
	eurdcna (P1)	Region 1	EURS-guided extrapolation
	eurdcra (P1)	Region 1	EURS-guided extrapolation
	erudcnsp (P2)	Region 2	Linear extrapolation or large-incidence aero extrapolation
	eurdcrsp (P2)	Region 2	Linear extrapolation or large-incidence aero extrapolation
	erudcnr (P1)	Region 2	Linear extrapolation or large-incidence aero extrapolation
	eurdcrr (P2)	Region 2	Linear extrapolation or large-incidence aero extrapolation
Dynamics	eurcmdyn (P2)	Region 2	EURS-guided extrapolation
	eurcnpbh (P2)	N/A	Extrapolation not viable for capturing stable-unstable breaks
	eurcrpbh (P1)	N/A	Extrapolation not viable for capturing stable-unstable breaks
	eurcnrbh (P2)	N/A	Extrapolation not viable for capturing stable-unstable breaks
	eurcrrbh (P2)	N/A	Extrapolation not viable for capturing stable-unstable breaks

3.5 STATIC AND DYNAMIC WIND TUNNEL TESTING REQUIREMENTS

The requirements for wind tunnel testing were developed based on data range, density, and accuracy requirements established for the moment parameters in a new EURS-like model. The ability to use analytic methods to provide the required accuracy levels when possible was included

in the development of these testing requirements. The capabilities of the wind-tunnel facility, test-data accuracy, model-component parts counts, and high-level test condition requirements (angle of attack, sideslip, and rate requirements) were included as well. With both statics and dynamics simulation model components requiring accurate data that cannot be developed by purely analytical means, both static and dynamic tests are required. To minimize costs, model re-use for both tests is assumed, and it is expected that a tunnel facility will be selected so both static and dynamic tests can be performed. The NASA LaRC 14x22 Subsonic Wind Tunnel is an example of a tunnel successfully used in the past for both static and dynamic wind-tunnel testing.

Balance accuracy and repeatability for static wind-tunnel testing are generally well understood. Both NASA and Boeing have successful experience testing at a variety of tunnels; inputs for static-testing accuracy requirements were sought from experienced NASA and Boeing engineers. A common reference cited and used extensively at Boeing and many test facilities is 'Low-Speed Wind Tunnel Testing' [7]. From this reference, the permissible measurement errors for a typical wind-tunnel test are outlined in table 3. By establishing that the moment parameters are the most critical for EURS-like models, trade-offs could be considered for drag, side-force, and lift accuracy. With no well-established repeatability standards for dynamic testing, maintaining the capabilities comparable to the facility used to develop the original EURS model is recommended.

Table 3. Static coefficient tolerance

Aerodynamic Coefficient	Permissible Measurement Error
CL	±0.002, or 0.25%
CD	±0.002, or 0.25%
Cm	±0.002, or 0.25%
Cn	±0.001, or 0.25%
Cl	±0.002, or 0.25%
CY	±0.002, or 0.25%

To provide data across an appropriate range of control-surface deflections, the accuracy conclusions discussed above were reviewed along with the EURS data to establish the minimum required set of control-surface deflections. Beyond the characteristics observed in the angle-of-attack and sideslip data ranges, linearity with control-surface deflection was considered to determine the requirements for intermediate control surface deflections. Table 4 summarizes the required control surface deflections that support a test plan providing test data to support the accuracy requirements of a new EURS-like model.

Table 4. Control deflections in degrees

Control Surface	Required Deflections / Settings
Stabilizer	-12, -8, 0, 4
Elevator	-30, -20, 0, 10, 20
Aileron (right)	0, ±10, ±20
Spoiler (right)	0, MID*, MAX
Rudder	0, 10, MAX
Flaps	Takeoff and landing

** Flaps-down testing only*

Requirements for angle of attack, sideslip, and rotational rate capabilities were established based on the required testing to support the accuracy requirements and are summarized below in tables 5 6. Testing should include lower angle-of-attack and sideslip conditions to anchor the test data to the original baseline model. Not all wind-tunnel sweeps will use the full range of angle of attack, sideslip, and rates, but these ranges are provided to ensure adequate balance capability for the range of required data.

Table 6 shows the combinations of reduced frequencies and oscillatory motion amplitudes used in the original EURS testing and the resulting range of reduced angular rates. It also includes the maximum oscillatory frequency for each axis, which would be important for future test planning. Actual values for reduced frequency and reduced angular rate would vary with changes in model geometry, test velocity, and amplitude of the oscillatory motion, but the values provided indicate the general capabilities required.

Table 5. Required range of angle of attack and sideslip testing

Angle of attack (deg.)	0, 6, 10, 12, 14, 16, 18, 20, 24, 28, 32, 36, 40, 45, 50, 55, and 60
Sideslip angle (deg.)	0, ±4, ±8, ±12, ±16, ±20, and ±30

Table 6. Required range of rate capabilities

Oscillatory Axes	Reduced Frequency Range, k	EURS Max. Oscillatory Frequency, Hz.	EURS Amplitude Range, (deg.)	Reduced Angular Rate Range, $\hat{\boldsymbol{p}}$, $\hat{\boldsymbol{q}}$, $\hat{\boldsymbol{r}}$
Pitch	0.0010–0.029	0.86	5 to 15	0.0008–0.0075
Roll	0.054–0.216	0.92	5 to 30	0.005–0.113
Yaw	0.055–0.215	0.86	5 to 30	0.005–0.113

3.6 WIND TUNNEL TEST PLANS

Detailed test plans were developed to provide adequate coverage of accurate test-based data that can be used as baseline datasets from which appropriate analysis techniques can be used to develop

future EURS-like models. Given the potential to develop future models over a range of configurations, multiple test options were considered with varying amounts of test data collected. The three options considered were:

> Option A—Provides test data to the minimum-required data boundaries with minimal reliance on extrapolation methods with appropriate data density. This option would be selected if the simulated stall-departure characteristics and motion parameters require a high level of accuracy and fidelity or if a significantly different aircraft configuration is being modeled (e.g., t-tail and blended-wing-body).
>
> Option B—Provides test data over the acceptable reduced data range and density and employs extrapolation techniques that are judged adequate for maintaining the prescribed model parameter accuracy requirements. This option would be selected if the simulated motion parameters need only capture the key stall-departure characteristics and individual departure aspects, and the aircraft configuration is similar to that modeled by the EURS.
>
> Option C—Provides test data with further reduced data range and density, and employs extrapolation and data-filling techniques that cannot be guaranteed to meet prescribed model-accuracy requirements. This option would risk a simulation that does not adequately capture the key stall-departure characteristics and individual departure aspects unless the airplane configuration modeled is extremely similar to that of EURS and its aerodynamics blend well with those of the EURS.

Which option is most appropriate to the development of a future EURS-like model would ultimately be a configuration-specific decision. With a reasonably similar configuration and expectations that precise stall-departure modeling can be sacrificed if key departure characteristics and aspects are captured, Option B would be the recommended basis for a test campaign. With increased experience in developing EURS-like models over a range of configurations, Option C could become more viable by providing a database of characteristics to account for configuration differences, including reasonable differences in wing and tail planform (aspect ratio, sweep, etc.) and control-surface positioning.

The test plans developed for each of the options are presented in tables 7–12; the test conditions are represented with an ‘A’, ‘B’, or ‘C’ to represent the three options discussed above. Static tests requirements are shown in terms of fixed sideslip and control surface positions at which angle-of-attack sweeps are performed. For each run, the sweep would go to the required angle-of-attack limit consistent with the planned extrapolation approach for the database development. One key place where the proposed test plans save significant test time relative to the EURS test campaign is by avoiding sideslip sweeps at fixed angle of attack; this is enabled by the course requirements for sideslip density. Dynamic test requirements are shown in terms of oscillation magnitudes and frequencies in each axis; the values are approximate based on the previous EURS development. Developers of future EURS-like models should review requirements to ensure that the range is applicable to the specific airplane being modeled.

Table 7. Static stability testing requirements

Alpha Sweep	STAB=0 / Elevator=0		
	Option A	Option B	Option C
@Beta Angles	0,±4,±8,±12,±16, +20, ±30	0,±4,±8,±12,±16	0,±8,±16

Table 8. Stabilizer and elevator effectiveness testing requirements

Alpha Sweep	Elevator				
@Stabilizer	20	10	0	-20	-30
-12	A/B/C	A/B	A/B/C	A/B	A/B/C
-8	A/B	A	A/B/C	A	A/B
0	A/B/C	A/B	Ref Cond.	A/B	A/B/C
4	A/B/C	A/B	A/B/C	A/B	A/B/C

Table 9. Aileron effectiveness test requirements

Alpha Sweep	Aileron Left / Right	
@Beta	0/±10	0 / ±20
0	A/B	A/B/C
±4	A/B	A/B
±8	A/B	A/B
±16	A/B	A/B/C
±30	A	A

Table 10. Spoiler effectiveness test requirements

Alpha Sweep	Right Spoilers Inboard / Outboard	
@Beta	MID/MID	MAX/MAX
0	A/B *(FD only)*	A/B/C
±16	A *(FD only)*	A
±30	A *(FD only)*	A

Table 11. Rudder effectiveness test requirements

Alpha Sweep	Rudder	
@Beta	10	MAX
0	A	A/B/C
±4	A	A
±8	A	A
±16	A	A
±30	A	A

Table 12. Dynamic stability test requirements

Pitch Axis	Amplitude, deg.		
@Freq, Hz	5	10	15
0.4	A	A	
0.6	A	A	
0.8	A	A	

Roll Axis	Amplitude, deg.		
@Freq, Hz	5	10	20
0.25		A	A
0.5	A/B/C		A
1.0	A/B/C	A/B/C	A

Yaw Axis	Amplitude, deg.		
@Freq, Hz	5	10	20
0.25			
0.5	A/B		
1.0	A/B	A/B	

Both static and dynamic test matrices described above were developed for flaps-up testing. The flaps-down model can use the reduced test matrices defined in Options B and C, with data acquired for a one-takeoff and one-landing flap deflection. This assumes that flap trends can be developed with interpolation techniques in the model blending stall and post-stall angle-of-attack range. It is recommended that an extra spoiler deflection is required to capture nonlinear trends with spoiler deflection, which can be more pronounced flaps-down. The deflection should be selected based on trusted baseline model trends. To estimate the required test time, it was assumed that the static-testing run rate is 2 runs per hour, and the dynamic testing run rate is 1.3 runs per hour. Furthermore, an 8-hour work day was assumed for these estimates. A summary of the testing required is provided in terms of run counts and estimated test times in tables 13 and 14. These data are used directly when estimating the costs of the wind-tunnel testing.

Table 13. Flaps UP run count comparison to the EURS test

	EURS		Option A		Option B		Option C	
	FUP	FDN	FUP	FDN*	FUP	FDN*	FUP	FDN*
Static stability (Long, Lat/Dir)	68	*Not Compiled*	12	18	9	10	5	10
Stab effectiveness	5		4	8	4	6	3	6
Elevator effectiveness	17		16	28	14	12	6	12
Aileron effectiveness	46		36	56	28	16	6	16
Spoiler effectiveness	13		5	20**	1	2	1	2
Rudder effectiveness	46		18	2	1	2	1	2
Dynamic stability	54		20	12	6	6	3	6
Totals			255		113		79	

** FDN – Flaps-down conditions for Takeoff and Landing configuration*

*** Flaps-down spoiler runs include an MID deflection.*

Table 14. Static and dynamic test summaries—test times (days)

	Option A		Option B		Option C	
	FUP	FDN	FUP	FDN	FUP	FDN
Static test time	6	8.5	3.5	3	1.5	3
Dynamic test time	3.5	2	1	1	0.5	1

3.7 COST ESTIMATES FOR EURS-LIKE SIMULATION DEVELOPMENT

The costs associated with developing new EURS-like simulation models is estimated by breaking down costs into three major components: wind-tunnel model design and fabrication, wind-tunnel test occupancy and support, and post-test analysis and simulation model-building. These estimates are based on the number of model parts, wind-tunnel facilities capable of this type of testing, and the test time, engineering time, and hourly rates for the tasks. The U.S. Government's General Services Administration "Contract-Award Labor Category" tool [5] was used for engineering labor rates. Using this tool to determine rates for engineers, labor rates ranged from as low as $170/hr to as high as $270, depending on the range of education and experience assumed; the mid-range value was $220.

3.7.1 Wind-Tunnel-Model Cost Estimates

The following ground rules were stipulated regarding the wind-tunnel-model costing effort for static and dynamic testing.

1. The model, if only one was fabricated, would be suitable for static and dynamic wind-tunnel testing.
2. The model(s) shall be unpowered.
3. The model(s) do not include pressure taps.

4. No credit for cost benefits of additive manufacturing techniques is considered.
5. The model(s) will include sufficient control surfaces for aerodynamic database developments (e.g., three position flaps, two position slats, ailerons, spoilers, rudder, movable horizontal tail, and elevator).
6. The model must be able to test up to 60º alpha and 30º beta; though at reduced dynamic pressure.

Rough order of magnitude cost estimates were sought from both within Boeing and from external organizations. None provided written estimates or hours because of the future nature of this exercise. Of those that gave rough estimates; the consensus was that a model such as the one described could be fabricated for approximately $400,000 in 2016 dollars.

3.7.2 Wind-Tunnel Test Costs

The NASA LaRC 14x 22 Subsonic Wind Tunnel is an example of a tunnel successfully used in the past for both static and dynamic wind-tunnel testing. According to NASA, the cost-per-tunnel occupancy hour is $3100/hour with an additional energy charge of $100/hour when the fan is running. It is assumed that fan-on time is approximately 50% of the test time, resulting in an approximate cost per hour of $3150/hour during active testing. The wind-tunnel occupancy costs are estimated by the test times for each testing option with the assumption that a fixed-model build-up time of 3 days, for which the base $3100/hour is applied. Assuming three engineering customers participated in supporting the test, the overall cost are summarized in table 15.

Table 15. Estimated wind-tunnel occupancy costs

	Option A	Option B	Option C
Wind-Tunnel Test Costs	$662,000	$328,000	$253,500

3.7.3 Potential Test Cost Savings

In addition to additive manufacturing techniques, there are other options to reduce cost that should be considered. One option to reduce cost would be to build a separate forced-oscillation model for testing in a small-scale water tunnel rather than a large wind-tunnel model capable of both static and dynamic testing. Boeing is exploring forced-oscillation wind-tunnel testing at the Flow Visualization Water Tunnel (FVWT). Forced-oscillation water-tunnel testing has the potential of reducing cost. Models for this facility, made from 3-D printed plastic, can be relatively inexpensive as well.

3.7.4 Post-Test Analysis Costs

Cost estimates for developing EURS-like models are based on expected times for post-processing of wind-tunnel data, data extrapolation and interpolation, any data blending/merging that is required across the datasets: baseline simulation, wind-tunnel, and EURS reference data. For model components that have robust wind-tunnel datasets, the task of developing model coefficient and increment tables from wind-tunnel data is well understood, including application of Reynolds Number adjustments (as appropriate), blending data into the flight-updated baseline simulation models, and adapting to its formats. A reduction in the amount of test data reduces the data-

processing time. However, the difficulty of integration of the data trends into an existing simulation model increases. The data integration task becomes more complex. The application of extrapolation, interpolation, and blending techniques becomes more difficult and time consuming when taking into account configuration differences of the airplanes modeled. Based on past experience in the development of the EURS model and other similar tasks, static model components are estimated to require approximately 3 man-weeks of effort, and dynamic model components are estimated to require approximately 4.5 man-weeks of effort when a robust set of wind-tunnel data is available and minimal analysis is required. On average, it is expected that analysis techniques to fill gaps in the wind-tunnel data would add approximately 3 man-weeks of effort to the development time for individual model components. Based on the model components being developed and the expected level of effort entailed, estimated analysis times and costs are provided in table 16. There are minor cost increases from Option B to C because of increased analysis difficulty and time required for the dynamic yaw characteristics and the interpolation and shaping within the bounds of the sparse data collected in both static and dynamic tests.

Table 16. Estimates for analysis required for EURS-like model development

	Option A	Option B	Option C
Statics Parameters	5 man-months	8 man-months	8.5 man-months
Dynamics Parameters	3 man-months	4 man-months	4.5 man-months
Total Labor	8 man-months	12 man-months	13 man-months
Total Labor Cost	$262,500	$405,000	$440,000

3.7.5 Net Costs of EURS-like Model Development

The net costs of developing EURS-like models with the options discussed is an aggregation of the model design and fabrication, wind-tunnel test costs, and post-test data processing, which includes analysis required to fill in any portions of the required dataset not captured by the wind-tunnel test program. Approximate costs for the three options are summarized in table 17. Although savings are available with Options B and C, the cost roll-up demonstrates that savings from the reduced wind-tunnel testing are partially offset by increased analysis costs. With small-to-moderate savings offered between Options B and C, the recommendation to use plan B for similarly configured airplanes remains until sufficient data are gathered across multiple configurations to build confidence in analysis techniques required to support Option C.

Table 17. Estimates of net cost to develop new EURS-like models

Program Costs	Option A	Option B	Option C
Test Model Construction	$400,000	$400,000	$400,000
Wind Tunnel Testing	$662,000	$328,000	$253,500
Simulation Model Development	$262,500	$405,000	$440,000
Total	$1,324,500	$1,133,000	$1,093,500

4. CONCLUSION

The ability to define stall departure in quantitative terms was the cornerstone of this project. It provided the means to achieve the principal goal of this project—the assessment of the level effort and cost to develop a simulation model for a similarly configured transport category airplane as that modeled by the NASA Enhanced Upset Recovery Simulation (EURS). Achieving this goal required a method to quantitatively categorize and define specific aspects of stall-departure characteristics using basic flight parameters, such as those found in flight data recorder, flight-test, and simulation data. Developing this method was the first objective of this project.

An extensive search of the public literature and engagement of the subject-matter experts at The Boeing Company revealed that no such method existed. However, there was sufficient insight gained and information gathered in this endeavor to develop such a method specifically for this project.

The Qualitative Stall Departure (QSD) Definition Tree method is a process in which a path along a logic-tree identifies patterns and relationships in the value, sign, and vector orientation of pertinent flight or simulation parameters. These patterns and quantitative relationships, and the logic paths traced throughout the time history of a stall departure, together characterize and define the individual aspects of the departure and the sequence in which they occur.

The second objective was to assess the capability of the EURS to reproduce any of the stall and post-stall departure characteristics defined via the QSD process. Analysis of a multitude of stall maneuvers in desktop and pilot-in-the-loop simulations revealed two major stall-departure characteristics: yaw departures and roll departures. Several individual aspects of these two departure characteristics were identified in the following combinations and sequence from the initial phase of the stall departure to its fully developed post-stall phase:

1. Initial stall phase nose-slice followed by stabilizing roll-off
2. Initial stall phase coordinated roll-off followed by opposite nose slice
3. Fully developed, post-stall phase, “hung” sideslip
4. Fully developed, post-stall phase, wing-rock in a slow, oscillatory spiral
5. Post-stall wing-rock followed by post-stall gyrations, never developing fully into a slow oscillatory spiral (roll math pilot OFF and yaw damper OFF)
6. Decay of lateral and directional control effectiveness
7. Commanded slow, oscillatory spiral/spin (full rudder hold)
8. Commanded falling leaf (full-forward column with full rudder)

Most of these stall-departure aspects, particularly those in their fully developed form, were the result of aggravating control inputs, held as long as 60 seconds. These control inputs drove the simulations far beyond the typically benign stall characteristics exhibited in nominal flight-test stall maneuvers, in which recovery is prompt and uneventful. Except for the initial nose-slice and roll-off departure aspects, the rest were present only in prolonged commanded deep-stall maneuvers at the aft-CG limit, holding the column at the aft stop.

The third objective was two-fold: to determine which parameters in the EURS aerodynamics model contributed to these individual departure aspects, and what degree of modeling accuracy was required to adequately simulate them.

First, individual components/parameters in the EURS aerodynamics model were correlated to each aspect of the stall and post-stall departure characteristics identified. This was achieved by assessing the effect on the defining QSD patterns and relationships for an individual aspect in a stall-departure simulation when the EURS component of each model parameter was deactivated individually and in its respective group. Each parameter was correlated with the individual stall-departure aspects by the magnitude of the deviations from its defining QSD patterns and relationships. The magnitude of these deviations was visually assessed and rated, and each EURS parameter was ranked high, medium, or low, based on these ratings. This method of rating the magnitude of the effect on the defining QSD patterns and relationships in a stall-departure simulation was used in all assessments of the simulation fidelity that followed. The visual ranking method and results were the basis for the development of a numerical ranking method in which the magnitude of the observed effects was scored numerically; each individual parameter was then quantitatively ranked by the total score of all the individual effects observed. Of the 40 EURS parameters, 8 were ranked high, 8 medium, and the rest low.

The number of EURS parameters required to provide adequate simulation fidelity was then determined using the inverse of the elimination process for the correlation and ranking of these parameters. Results showed that simulation fidelity was unacceptable with the high-rank parameters activated alone and the rest deactivated. Activating both high- and medium-rank parameters did not sufficiently improve simulation fidelity. Some of the low-rank parameters had to be activated along with the high- and medium-rank parameters to achieve an acceptable level of simulation fidelity. The final number of required parameters increased to 21, all of them moment parameters.

The final step in achieving the third objective of this project focused on three major factors affecting modeling accuracy: data range, density, and value. Reductions in data range and density and the tolerance to data value inaccuracies were explored. Results showed that the data range and density of these 21 high-impact parameters could be reduced to the following required minimums without degrading simulation fidelity:

- Range in angle-of-attack was up to 60º (reduced from 90º in the EURS).
- Range in sideslip was out to ±30º (reduced from ±45º in the EURS).
- Range in nondimensional roll and yaw rotational rates was up to ±0.075 (reduced from ±0.110 in the EURS).
- Range in nondimensional pitch rate was to ±0.005 (reduced from ±0.0076 for the EURS).
- Density in sideslip data of every 4º (reduced from every 4 degrees for the EURS).

Angle-of-attack density in either the static or dynamic parameters and rate density on the latter should be the same as that in the EURS model, as reflected in the recommended test plans.

The degree of tolerance to data value inaccuracies would determine the potential for extrapolation to the required-minimum ranges listed above, from a reduced region of accurate data within the required-minimum-range boundaries. Results showed that comparable simulation fidelity with up

to a ±10% inaccuracy in the model data values was acceptable at the bounds of the required-minimum ranges if data accuracy is maintained up to the bounds of Region 1, as defined in figure 32.

Insight into the relationship between stall and post-stall departure simulation and the extent and accuracy of the aerodynamics modeling required were instrumental in achieving the fourth objective and principal goal of this project: To develop a cost-effective plan for acquiring the aerodynamic data required to develop a simulation comparable to the EURS.

A search for accurate analytical methods revealed that the bulk of the data will necessarily have to be acquired through the same type of wind-tunnel testing as for the EURS development, although not as extensive. Three test options were considered, each developed by trading cost and data accuracy within the prescribed requirements set above, which include extrapolation through available analytical methods or guided by EURS-model trends and engineering judgment.

Option A— Provides test data to the minimum-required data boundaries with minimal reliance on extrapolation methods with appropriate data density. This option would be selected if the simulated stall-departure characteristics and motion parameters require a high-level of accuracy and fidelity.

Option B—Provides test data over the acceptable reduced data range and density, and employs extrapolation techniques that are judged adequate for maintaining the prescribed model-parameter accuracy requirements. This option would be selected if the simulated stall-departure characteristics and motion parameters need only capture the key stall-departure characteristics and individual departure aspects with an acceptable level of accuracy and fidelity.

Option C—Provides test data with greatly reduced data density and employs extrapolation and data-filling techniques that cannot be guaranteed to meet prescribed model-accuracy requirements. This option would risk a simulation that does not adequately capture the key stall departure characteristics and individual departure aspects unless the airplane configuration modeled is extremely similar to that of EURS, and its aerodynamics blend well with those of the EURS.

When selecting one of these options, the cost and extent of the wind-tunnel testing should not be the primary factor. Depending on which test option is selected, there are different levels of effort for post-test processing analysis, data extrapolation, and aerodynamics model-building. Test and post-processing cost savings can be achieved by reducing test matrix size. However, these cost savings may not be sufficient to offset the added cost of expanded data extrapolation and interpolation analysis to fill data gaps and the increased complexity in the model building required to blend test and extrapolated datasets.

The test option recommended (Option B) relies on analytical methods based on simple separated-flow aerodynamic theory with limited knowledge of the EURS aerodynamics when extrapolating beyond the reduced-data range for acceptable extrapolation. This option provides acceptable confidence in the data buildup from the reduced accurate test-data range to the minimum-required range when considering the accuracy requirements. All options from A through C are viable, except possibly Option C because the level of modeling accuracy and simulation fidelity may be compromised.

The conclusions and recommendations put forth here can serve as a guide in developing the aerodynamics for flight simulators capable of sufficiently accurate representations of the stall and post-stall departure characteristics of a conventional twin-jet transport category airplane.

5. REFERENCES

1. Boeing Commercial Airplanes. (2011). Statistical Summary of Commercial Jet Airplane Accidents, World Wide Operations, 1959–2010.

2. NASA Report. (2010). Aircraft Loss-of-Control Accident Analysis. Retrieved from https://ntrs.nasa.gov/archive/nasa/casi.ntrs.nasa.gov/20100030600.pdf

3. FAA Report. (2010). Concept of Operations for the Next Generation Air Transportation System. Retrieved from http://www.dtic.mil/dtic/tr/fulltext/u2/a535795.pdf

4. AIAA Report. (2004). Defining Commercial Transport Loss-of-Control: A Quantitative Approach. (AIAA 2004-4811).

5. AIAA Report. (1980). Stall/Spin Flight Results for the Remotely Piloted Spin Research Vehicle. (A80-45862).

6. Chakraborty, A., Seiler, P., Balas, G. J. Susceptibility of F/A-18 Flight Controls to the Falling Leaf Mode: Linear Analysis. *Journal of Guidance, Control and Dynamics, 34*(1) 57–72.

7. Barlow, J. B., Rae, W. H., Pope, A. (1999). *Low-Speed Wind Tunnel Testing* (3rd ed.), Hoboken, NJ: Wiley-Interscience.